Advances in Colloid and Interface Science 358 (2026) 104049

Contents lists available at ScienceDirect

Advances in Colloid and Interface Science

journal homepage: www.elsevier.com/locate/cis

Hollow microgels: Interplay of structure, mechanics, and transport

Chandeshwar Misra [a,*], Alan O. Francisco-Mejia [a], Walter Richtering [a], Jérôme J. Crassous [a,b,**]

[a] Institute of Physical Chemistry, RWTH Aachen University, Landoltweg 2, 52074, Aachen, Germany
[b] Jülich Centre for Neutron Science (JCNS-1), Forschungszentrum Jülich GmbH, Wilhelm-Johnen-Straße, 52425 Jülich, Germany

ARTICLE INFO

Keywords:
Hollow microgels
Responsive microgels
Soft colloids
Polymer networks
Shell mechanics
Interfacial behavior
Encapsulation
Transport

ABSTRACT

Responsive hollow nano- and microgels, cross-linked polymer networks containing a solvent-filled cavity, have attracted significant interest in both fundamental science and emerging technologies. The presence of these internal cavities imparts enhanced softness and deformability, enabling pronounced and tunable size and shape transformations in response to external stimuli. As a result, these systems are particularly well suited for biomedical applications such as drug delivery, controlled release, and encapsulation. By tuning synthesis conditions and incorporating appropriate functional moieties, hollow microgels can be engineered to respond to environmental triggers, including pH, temperature, and ionic strength. This review summarizes recent advances in the synthesis, properties, and applications of hollow nano- and microgels, with a particular focus on their mechanical and interfacial behavior. When subjected to external stresses, such as osmotic pressure, these systems can undergo significant shape transformations, including deswelling via inward network reconfiguration or buckling instabilities, depending on their size and core-to-shell ratio. At interfaces and under confinement, their high deformability enables complex morphological adaptations that govern their interactions and assembly. We further discuss these behaviors in the context of theoretical and computational studies. Finally, emerging features such as shape anisotropy and their implications for future applications are highlighted.

Contents

1. Introduction 2
2. Synthesis of hollow responsive microgels 3
3. Building up responsivity 6
4. Hollow nano/microgels under stress: Deswelling or buckling? 7
5. Interfacial assembly: Spreading or No spread? 11
6. Influence of shape anisotropy 14
7. Potential applications of hollow microgels 15
8. Conclusions and future directions 17
CRediT authorship contribution statement 18
Declaration of Generative AI and AI-assisted technologies in the writing process 18
Declaration of competing interest 18
Acknowledgments 18
Data availability 18
References 18

* Corresponding author.
** Corresponding author at: Jülich Centre for Neutron Science (JCNS-1), Forschungszentrum Jülich GmbH, Wilhelm-Johnen-Straße, 52425 Jülich, Germany.
E-mail addresses: misra@pc.rwth-aachen.de (C. Misra), crassous@pc.rwth-aachen.de (J.J. Crassous).

https://doi.org/10.1016/j.cis.2026.104049
Received in revised form 4 September 2026
Available online 12 September 2026
0001-8686/© 2026 The Authors. Published by Elsevier B.V. This is an open access article under the CC BY license (http://creativecommons.org/licenses/by/4.0/).
Open access funding enabled and organized by Projekt DEAL.

1. Introduction

Microgels are soft, three-dimensional cross-linked polymer networks swollen in a good solvent, typically water [1–3]. Their widespread use stems from their remarkable chemical versatility, which enables the incorporation of diverse functional moieties, as well as their high loading capacity arising from their swelling properties. These features, combined with their intrinsic softness and deformability, make microgels attractive for a wide range of applications, including drug delivery systems [4–7], sensors [8,9], actuators [10,11], and smart emulsion stabilizers [3,12,13].

Beyond their functional versatility, microgels are canonical model systems for soft colloids, as their physicochemical nature lies at the interface between polymers, surfactants, and conventional hard colloids. Their softness arises from their ability to reversibly swell and deswell in response to external stimuli such as temperature [2,14,15], pH [16–19], and ionic strength [20,21], as well as from their capacity to deform, facet, and interpenetrate under confinement or at high concentrations as discussed in recent reviews and experiments [22,23]. These properties enable dense packings beyond the random close packing of hard spheres and promote defect healing in crowded environments [24–26].

These behaviors are strongly governed by microgel size and internal architecture. As will be discussed in this review, introducing a solvent-filled cavity within the microgel structure adds an additional level of complexity, as the relative dimensions of the cavity and shell thickness critically influence the deformability and mechanical response of these systems. Building on these features, hollow microgels represent a particularly intriguing extension of soft colloidal systems, as they introduce an additional structural degree of freedom in the form of a solvent-filled cavity. Distinguished from conventional microgels by this internal void, these systems exhibit unique mechanical and physicochemical properties that are not accessible in homogeneous polymer networks [27–31]. A schematic representation of the hollow microgel geometry is shown in Fig. 1, highlighting the characteristic structural parameters.

In contrast to other hollow soft materials such as vesicles [32,33], liposomes, and polymerosomes [34,35], hollow microgels are cross-linked, porous elastic shells that behave as soft solids rather than fluid membranes. This fundamental difference in internal structure gives rise to distinct mechanical responses: while bilayer systems deform primarily through smooth, area-preserving membrane fluctuations governed by bending rigidity, hollow microgels can sustain shear stresses and undergo pronounced shape transformations, including swelling, deswelling, wrinkling, and buckling under osmotic pressure. Their porous and permeable polymer network allows rapid solvent and solute exchange with the surrounding medium, so that environmental changes (e.g., pH, temperature, or ionic strength) directly affect the osmotic balance and polymer–solvent interactions within the shell. As a result, their swelling state, mechanical properties, and interparticle interactions can be continuously tuned. The presence of an internal cavity not only enhances their effective softness by enabling polymer rearrangement within the shell, but also provides additional volume for encapsulation and transport of guest molecules. Consequently, hollow microgels have attracted increasing interest for applications ranging from drug delivery and encapsulation to membrane technologies and soft templating [36–39].

Given the broad range of applications and the sensitivity of their properties to internal structure, the controlled synthesis of hollow microgels has become a central aspect of current research. A variety of synthetic strategies have been developed, which differ not only in their chemical approach but also in the size range, structural precision, and scalability of the resulting systems. Among these, sacrificial templating remains the most widely used method, relying on either soft [40,41] or hard templates [42,43] that are subsequently removed to generate a hollow architecture. This approach offers a high degree of control over particle size and shell thickness, particularly when using monodisperse inorganic templates such as silica. However, it typically involves multistep procedures and can present challenges in template removal and purification. Alternative strategies, including microfluidic approaches, inverse emulsions, and batch or precipitation polymerization, provide complementary advantages [44–47]. Microfluidic techniques enable the production of well-defined, often larger microgels with precise control over geometry, whereas bulk synthesis routes are more scalable but may yield less well-defined internal structures. As a result, the choice of synthesis method is closely linked to the targeted size regime and level of structural control. Importantly, these differences also determine the experimental approaches available to probe their properties. Nanoscale systems are typically investigated using scattering techniques, providing averaged structural information, whereas larger, fluorescently labeled microgels can be directly visualized in situ, enabling real-time observation of deformation, interfacial behavior, and collective dynamics. Finally, emerging challenges in the field include the controlled synthesis of anisotropic hollow microgels, which opens new opportunities for tailoring mechanical response and directional interactions in soft matter systems.

The presence of an internal cavity has profound consequences for the behavior of hollow microgels in dense environments, where mechanical interactions dominate. In contrast to conventional microgels, their compressibility is governed not only by the network elasticity but also by the ability of the polymer shell to rearrange into the internal void. As a result, the cavity has been shown to have a stronger impact on the mechanical response than variations in cross-linking density alone, leading to significantly enhanced deformability [48–50]. Under external osmotic pressure, this additional degree of freedom gives rise to distinct deformation pathways. Hollow microgels can either deswell through inward redistribution of the polymer network or undergo mechanical instabilities such as buckling, depending on their size and shell thickness [28,51]. More generally, for spherical hollow microgels, the ratio between cavity size and shell thickness, together with the elastic properties of the shell set by the cross-linking density, are key parameters governing their mechanical response. At the nanoscale, their high compressibility effectively reduces the occupied volume fraction in dense suspensions, increasing configurational entropy and thereby suppressing crystallization [26,49]. At larger length scales, the mechanical response becomes even more striking: microscale hollow microgels have been observed to undergo pronounced buckling transitions, forming anisotropic, bowl-like structures above a critical osmotic pressure [28,51]. Such shape transformations arise from instabilities of the thin elastic shell and highlight the solid-like character of these systems. Consistently, recent simulations demonstrate that sufficiently large hollow microgels can exhibit self-induced buckling even in dense dispersions, further emphasizing the role of geometry and confinement in controlling their deformation behavior [50]. Despite these advances, a comprehensive understanding of how the overall particle size influences the build-up of osmotic pressure, and thereby the competition between deswelling, faceting, and buckling, remains an open question.

The behavior of hollow microgels at fluid interfaces further highlights the importance of their internal architecture and enhanced deformability. Upon adsorption, microgels undergo significant shape changes, spreading and flattening at the interface to reduce interfacial energy. In hollow systems, this deformation is amplified by the presence of the internal cavity, which facilitates polymer redistribution within the shell and enables more pronounced shape adaptation compared to homogeneous microgels [52,53]. However, even for conventional microgels, the extent of interfacial deformation is not yet fully understood and remains an active area of research. In hollow microgels, this complexity is further increased by the interplay between cavity size, shell thickness, and elastic properties, which govern the balance between interfacial tension and mechanical resistance. Recent work highlights that microgel geometry plays a decisive role in interfacial behavior. Despite their high deformability, hollow microgels do not necessarily fully flatten [51], and a range of morphologies can

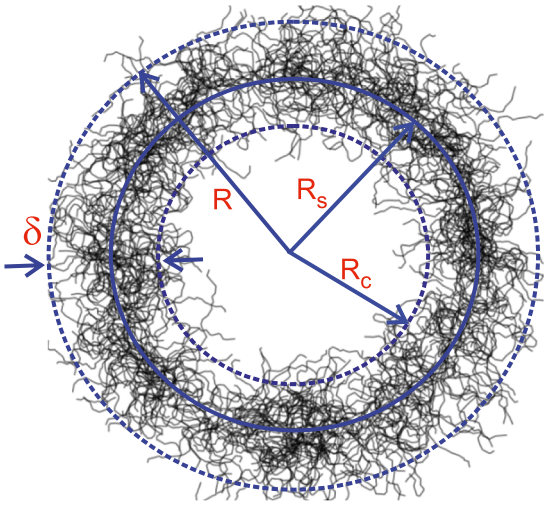

Fig. 1. Schematic illustration of a hollow microgel. The parameters R, R_s, R_c, and δ represent the total radius of the microgel, average radius, cavity radius, and shell thickness, respectively.

emerge depending on their structure and size [54]. Notably, capillary-interaction-driven self-assembly has been observed in anisotropic systems, underscoring the combined influence of shape, size, and internal architecture on interfacial organization [55,56]. Overall, these systems provide a powerful platform to explore the coupling between elasticity, geometry, and interfacial forces, although a predictive understanding of their deformation and assembly remains an open challenge.

In this review, we present recent advances in the field of hollow nano- and microgels, with a focus on how their internal architecture governs their physical properties and functional behavior. We first discuss the main synthetic strategies used to design hollow microgels, highlighting the key parameters that control their size and internal structure. We then examine their responsiveness to external stimuli, followed by a discussion of their mechanical behavior in crowded environments, where osmotic pressure, confinement, and particle interactions lead to pronounced shape transformations such as deswelling and buckling. Particular attention is given to their behavior at fluid interfaces, where their enhanced deformability and internal geometry give rise to complex interfacial morphologies and assembly pathways. Finally, we address emerging directions, including anisotropic hollow microgels and their potential for tailoring interfacial and bulk properties. Throughout the review, experimental findings are discussed alongside theoretical and computational insights to provide a coherent physical picture of these systems.

2. Synthesis of hollow responsive microgels

The synthesis of hollow microgels plays a central role in determining their dimensions, internal architecture, and consequently their mechanical and functional properties. A variety of synthetic approaches have been developed, including sacrificial templating, microfluidic techniques, dispersion-based methods, layer-by-layer assembly, and in silico strategies. These approaches differ significantly in terms of size range, structural control, scalability, and achievable geometries. Among them, sacrificial templating remains the most widely used method, owing to its versatility and ability to produce well-defined hollow structures with tunable size and shell thickness. Other approaches provide complementary advantages and are particularly suited to specific size regimes or functionalities.

It is important to note that these different synthetic approaches are often built upon common polymerization mechanisms, which largely determine the accessible size range and structural characteristics of the resulting microgels. In particular, sacrificial templating strategies frequently rely on seeded emulsion or seeded precipitation polymerization to form the microgel shell. More generally, a useful guideline is that the characteristic size of the resulting particles increases with the polymerization approach: emulsion polymerization typically yields the smallest systems, followed by precipitation polymerization, dispersion polymerization, and finally microfluidic techniques, which allow access to the micrometer regime. This provides a useful framework for understanding the strengths and limitations of the different synthesis routes discussed below.

Sacrificial template. Sacrificial templating is the most widely used strategy for producing hollow microgels and has been extensively employed by several groups [27,28,57–59]. In this approach, a core particle is first coated with a cross-linked polymer shell, after which the core is selectively removed to generate a hollow structure. This method is particularly powerful, as it enables independent control over particle size, shell thickness, and internal architecture.

A wide range of sacrificial templates has been explored. Among hard templates, inorganic silica particles remain the most commonly used due to their narrow size distribution, commercial availability across a broad size range, and well-established synthesis protocols. Beyond silica, other colloidal systems such as carbon nanospheres, metal nanoparticles, and metal oxide particles have also been employed to generate hollow architectures [59,60]. The choice of template directly impacts both the achievable size range and the removal strategy, as well as the final structural definition of the cavity. The fabrication of hollow microgels using hard templates typically involves four key stages (Fig. 2A): synthesis of monodisperse core particles (e.g., via the Stöber method [61] or using commercial colloids), surface functionalization-commonly with 3-(trimethoxysilyl)propyl methacrylate (MPS)—to introduce polymerizable groups, formation of a cross-linked polymer shell (often via precipitation polymerization), thereby yielding a core–shell microgel, and finally removal of the core, typically by dissolution in alkaline solutions such as NaOH. Each of these steps plays a critical role in defining the final microgel properties, particularly the grafting density, shell integrity, and mechanical response. Representative microscopy images of core–shell and hollow microgels are shown in Fig. 2B–D.

In contrast, soft sacrificial templates provide an alternative route based on degradable polymer cores [40,41,62–64]. A representative strategy employs PNIPAM cores crosslinked with degradable crosslinkers such as N,N′-(1,2-dihydroxyethylene)bisacrylamide (DHEA), followed by the formation of a non-degradable shell (Fig. 2E). The core is subsequently removed via selective cleavage of the degradable crosslinker, for instance by oxidation with sodium periodate ($NaIO_4$), leading to fragmentation of the network and diffusion of soluble polymer segments out of the particle. Compared to hard templating, soft templating approaches offer milder processing conditions and avoid the use of strongly basic or acidic treatments. However, they generally provide less precise control over cavity definition and shell uniformity, as partial material loss and incomplete removal of polymer fragments can lead to lower effective crosslinking densities and more diffuse internal interfaces. Experimentally, this is reflected in increased swelling ratios and enhanced deswelling amplitudes compared to their core–shell precursors, indicating a softer and more deformable structure.

Overall, sacrificial templating—whether based on inorganic or polymeric cores—provides a versatile route to hollow microgels with tunable internal architecture. While hard templates offer superior control and monodispersity, soft templates enable access to alternative structures under milder conditions. Importantly, both approaches allow independent tuning of cavity size and shell thickness, which, as discussed in the following sections, are key parameters governing the mechanical response and interfacial behavior of hollow microgels.

Microfluidics. Microfluidic techniques provide a powerful route to fabricate hollow microgels with exceptional control over size, morphology, and internal architecture [65–67]. In contrast to bulk synthesis

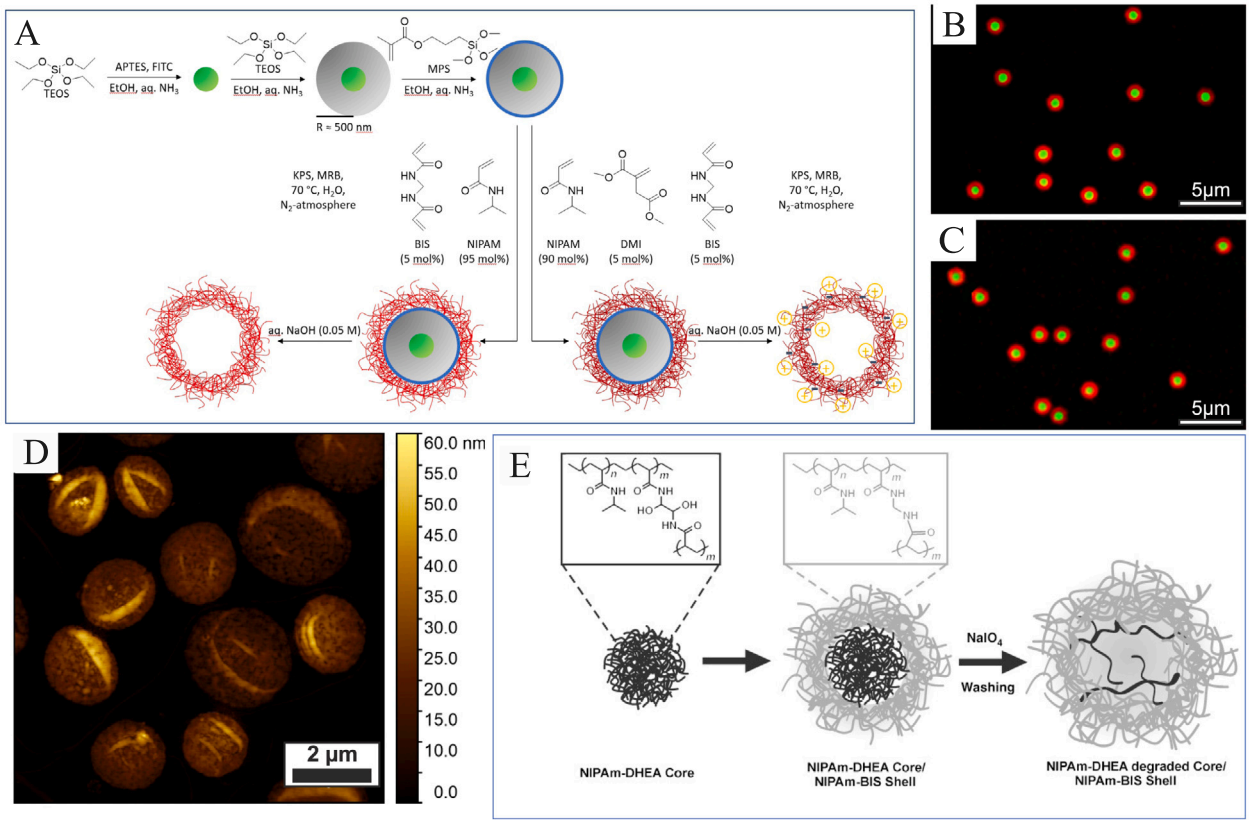

Fig. 2. (A) Schematic of the synthesis of hollow microgel, including preparation of silica templates, modification of silica surface, microgel shell polymerization, and silica core dissolution. Confocal micrographs of (B) neutral core–shell and (C) charged core–shell PNIPAM microgels. (D) Atomic force microscopy images of neutral hollow microgels. Adapted with permission from Ref. [28]. (E) Schematic illustration of the preparation of hollow microgel particles using soft-degradable cores.
Source: Adapted with permission from Ref. [40].

methods, they enable the generation of highly monodisperse double or multiple emulsions that serve as well-defined templates for subsequent polymerization. A key feature of microfluidic approaches is that they typically produce particles in the micrometer size range, which allows direct visualization by optical and confocal microscopy. However, this also implies that these systems lose their Brownian character, leading to negligible diffusion and pronounced sedimentation effects, which must be considered when interpreting their behavior.

A representative example was reported by Kim et al. [46], who employed a capillary-based microfluidic device to produce microgel shells via the formation of double emulsion droplets (Fig. 3A–C). In this approach, three fluid streams are combined: an outer continuous phase (typically oil), a middle aqueous phase containing monomers such as N-isopropylacrylamide (NIPAM), crosslinkers (e.g., BIS), and functional comonomers (e.g., METAC, allylamine), and an inner aqueous phase containing the initiator (APS). Controlled flow of these phases leads to the formation of uniform core–shell droplets, which are subsequently polymerized via a redox reaction triggered by diffusion of the accelerator between phases. Removal of the inner phase yields hollow microgel shells with well-defined geometry. While this double emulsion approach offers precise control over particle size and shell thickness via flow-rate tuning, maintaining a homogeneous shell thickness remains challenging in practice. In particular, density mismatch between the different phases can lead to off-centered cores and asymmetric shells (see inset of Fig. 3A), resulting in variations in local shell thickness. Although often considered a limitation, such asymmetry can also be exploited to direct deformation pathways or preferential degradation of the shell, providing additional opportunities to tailor the mechanical response of the system. Microfluidic approaches also enable direct investigation of thermoresponsive behavior. Measurements of inner and outer radii as a function of temperature (Fig. 3C) show that both decrease upon heating, reflecting the collapse of the polymer network. Interestingly, while the shell continues to shrink at elevated temperatures, the core volume remains relatively stable, suggesting reduced permeability of the densified shell. This highlights the ability of microfluidically produced systems to decouple shell mechanics from internal volume, providing a useful platform for studying transport and confinement effects.

Despite these advantages, microfluidic techniques are typically restricted to larger particles, generally in the micrometer to tens-of-micrometers size range (approximately 1–100 µm, depending on the device geometry and flow conditions), and require relatively complex setups. While inherently continuous, and thus in principle scalable through parallelization, their practical implementation at large scale remains challenging compared to bulk synthesis methods.

Layer-by-layer assembly. Layer-by-layer (LbL) assembly has emerged as a versatile strategy for constructing hollow polymeric shells through the sequential deposition of functional layers onto sacrificial templates [44,45]. This approach enables the incorporation of a wide range of materials, including polymers, peptides, oligonucleotides, and inorganic nanoparticles, and can rely on various interactions such as electrostatics, hydrogen bonding, host–guest interactions, or covalent coupling [68–71]. In the context of thermoresponsive systems, Huang et al. [72] demonstrated the fabrication of PNIPAM-based microcapsules using a covalent LbL approach based on click chemistry (Fig. 3D). In this method, azido- and acetylene-functionalized PNIPAM copolymers are sequentially assembled on silica templates, forming multilayered shells that are subsequently released by core dissolution

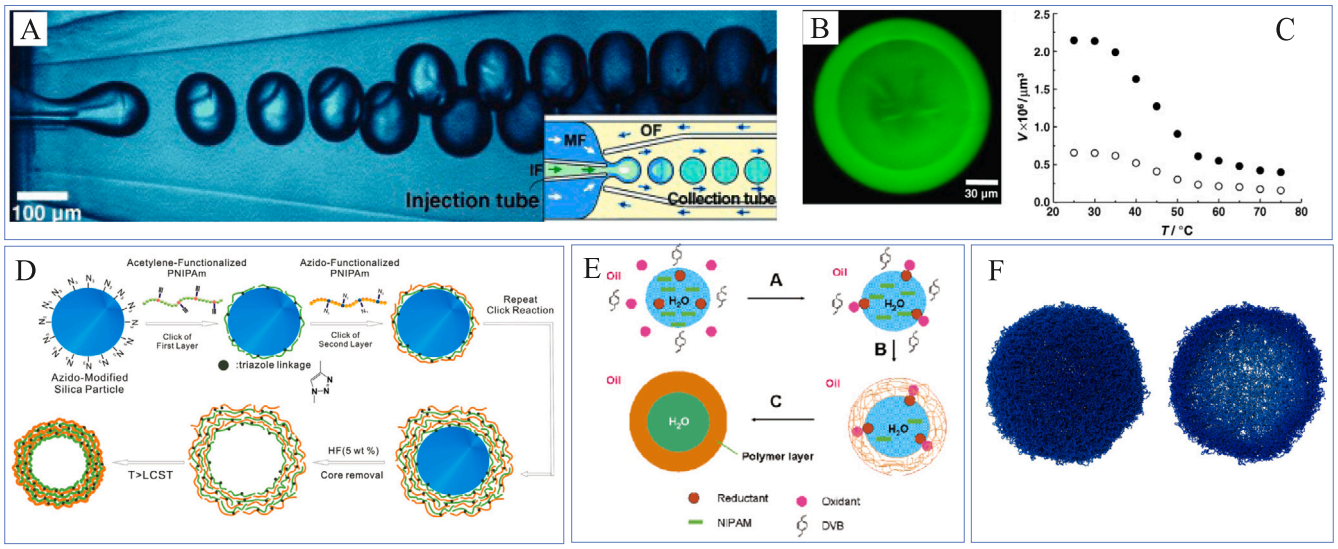

Fig. 3. (A) Formation of pre-microgel drops in a capillary microfluidic device. The inset shows the geometry of the microfluidic device. (B) Fluorescence micrograph of the FITC-labeled microgel shells. (C) Volume changes of the overall core–shell PNIPAM microgel (•) and its internal voids (○) as a function of temperature. Reproduced with permission from Ref. [46]. (D) Schematic representation of the production of covalently stabilized thermoresponsive microgels using layer-by-layer assembly and click chemistry. Reproduced with permission from Ref. [72] (E) Synthesis protocol for thermoresponsive hollow microgels via dispersion polymerization. This figure was reproduced with permission from [47]. (F) Simulation snapshots of a full (left) and cross-section of the hollow microgel in the in silico synthesis procedure.
Source: Adapted with permission from Ref. [51].

using hydrofluoric acid. The resulting capsules exhibit thermoresponsive behavior, as reflected by changes in size and shell thickness across the volume phase transition temperature.

However, it is important to note that LbL-derived hollow structures differ fundamentally from hollow microgels. In contrast to microgels, which consist of a three-dimensional cross-linked polymer network, LbL systems typically form thin polymer shells with limited network connectivity and often rely on interfacial assembly rather than bulk gelation. As a result, their mechanical properties, permeability, and deformation behavior are governed by shell mechanics rather than bulk network elasticity, bringing them closer to polymer capsules than to conventional microgels. Despite these differences, LbL approaches remain highly relevant, as they provide precise control over shell composition, thickness, and functionality. This makes them particularly attractive for applications requiring well-defined barrier properties and tunable permeability.

Dispersion polymerization. Dispersion-based approaches have also been employed to synthesize hollow microgels [47,73,74]. In contrast to templating strategies, these methods do not rely on a predefined core, but instead generate hollow structures directly during the polymerization process. As such, the formation of the internal cavity is intrinsically coupled to the kinetics of nucleation, phase separation, and network formation. A representative example was reported by Sun et al. [47], who developed a one-pot in situ polymerization method to produce thermoresponsive hollow microgels via interfacial polymerization (Fig. 3E). In this approach, NIPAM monomers are dissolved in an aqueous phase and emulsified in an organic solvent such as toluene to form a water-in-oil (W/O) dispersion, typically stabilized by low-HLB surfactants (e.g., sorbitan monooleate). The resulting droplets, with sizes on the order of 1–3 μm, act as transient compartments in which structure formation occurs. Polymerization is initiated at the oil/water interface using a redox system (e.g., benzoyl peroxide (BPO) and tetraethylene-pentamine (TEPA)), which generates radicals upon diffusion of the components to the interface. Importantly, polymerization is carried out above the volume phase transition temperature (VPTT) of PNIPAM, where the polymer becomes hydrophobic and is therefore confined to the interface. This leads to the progressive formation of a crosslinked shell, while the interior remains polymer-poor, ultimately resulting in a hollow structure. In this sense, the cavity is not templated but develops during the synthesis process.

While this approach enables relatively straightforward and potentially scalable production of hollow microgels, the resulting particles typically exhibit broader size distributions compared to templating or microfluidic methods. Parameters such as emulsion stability, droplet size distribution, agitation conditions, and reactant concentrations play a critical role in determining the final particle characteristics. As a result, these methods offer less precise control over cavity size and shell thickness, but remain attractive for producing hollow microgels in batches in a single-step process with relatively simple experimental setups.

Hollow microgels *in silico*. In silico approaches have become essential tools for investigating the structure and mechanics of hollow microgels, providing access to microscopic details that are difficult to probe experimentally [51,53,75,76]. A variety of modeling strategies have been developed, which differ significantly in how the internal network architecture is represented. Early approaches often relied on idealized network structures, such as diamond-like lattices or regular polymer networks [22]. These models provide well-defined and highly controlled architectures, allowing systematic investigation of elasticity, swelling, and deformation. However, they do not capture the structural heterogeneity and disorder that are characteristic of experimentally synthesized microgels.

More recent models have therefore focused on generating disordered networks via in silico synthesis protocols, typically based on the self-assembly of patchy particles representing monomers and crosslinkers [75,76]. These approaches naturally lead to heterogeneous internal structures and can incorporate features such as radial density gradients, which are commonly observed in real microgels [75,77]. Extensions of these methods have been used to generate hollow architectures by introducing confined regions [51] or a microgel templating approach. In this context, the resulting hollow microgels exhibit structural and mechanical properties strongly influenced by the interplay among network heterogeneity, cavity size, and shell thickness, consistent with experimental observations.

A key limitation of simulation approaches lies in the accessible size range. Due to computational constraints, simulated microgels are typically much smaller than their experimental counterparts, necessitating significant coarse-graining. As a result, effective interaction potentials (e.g., bead–spring models such as the Kremer–Grest framework) must be carefully tuned to reproduce experimentally relevant behavior. This raises important questions regarding the transferability of model parameters and the quantitative comparison between simulations and experiments. Despite these limitations, simulations provide invaluable insight into the fundamental mechanisms governing swelling, deformation, and buckling of hollow microgels. In particular, they allow systematic exploration of parameters such as network topology, crosslinking density, and cavity geometry, thereby complementing experimental studies and contributing to a more comprehensive understanding of structure–property relationships in these systems.

The different synthetic strategies discussed above provide access to hollow microgels with a wide range of internal architectures and structural complexities. These methods can also be compared in terms of the degree to which shell thickness and cavity size can be independently controlled. In sacrificial templating, the cavity size is primarily determined by the template diameter, whereas the shell thickness is governed by the monomer and crosslinker concentrations, polymerization time, and grafting density at the core surface. In contrast, microfluidic methods tune the shell thickness through the relative flow rates of the droplet-forming phases, although shell asymmetry may arise from core displacement. Layer-by-layer assembly provides stepwise control over the thickness by varying the number of deposited layers, whereas dispersion-based methods offer less direct control because the hollow structure is formed through coupled phase separation and polymerization. These differences are important because the shell thickness, crosslinking density, and cavity size determine the swelling, deformability, permeability, and mechanical response of hollow microgels, which are discussed in the following sections.

3. Building up responsivity

Responsiveness to external stimuli is a defining feature of microgels and underpins both their fundamental interest and technological relevance. In conventional microgels, this behavior is typically governed by a relatively homogeneous volume phase transition (VPT), resulting from changes in polymer–solvent interactions, as exemplified by PNIPAM and PNIPMAM systems [2].

In hollow microgels, however, the presence of a cavity introduces an additional degree of freedom, leading to a spatially heterogeneous response. Upon core removal, the final structure is determined by a balance between shell elasticity, crosslinking density, and osmotic pressure. As a result, swelling and deswelling processes involve not only network collapse but also solvent transport, permeability of the shell, and redistribution of polymer chains within the cavity. In the following, we discuss how hollow microgels can be engineered to respond to temperature, pH, and ionic strength, and how their internal structure can be characterized.

Characterization of responsive behavior. The investigation of responsive hollow microgels relies on complementary experimental techniques, whose applicability depends strongly on particle size. Large microgels can be directly visualized in situ using optical or fluorescence microscopy, super-resolution microscopy, providing access to shape changes, deformation, and internal restructuring [28,51,78–80]. In contrast, smaller systems are typically characterized by dynamic light scattering (DLS), which provides information on the overall hydrodynamic size and diffusion [22].

To probe internal structure and density distributions, scattering techniques such as small-angle X-ray scattering (SAXS), small-angle neutron scattering (SANS), and static light scattering (SLS) are widely employed. In particular, SANS is highly powerful for multicomponent systems due to the possibility of contrast variation, enabling independent probing of shell and cavity regions [26,28,49,51,81]. These methods are essential for resolving features such as density gradients, shell thickness, and cavity evolution, which are not directly accessible from size measurements alone [22]. In addition, real-space imaging techniques such as cryogenic electron microscopy (cryo-TEM) provide direct access to the internal structure of smaller hollow microgels in their hydrated state, enabling visualization of cavities and polymer distribution at the nanoscale. Atomic force microscopy (AFM), including advanced modes such as stiffness tomography, further allows probing of local mechanical properties and spatial variations in elasticity within individual particles. Together, these approaches provide complementary insights into both the structural and mechanical heterogeneity of responsive hollow microgels [28,82,83].

Thermoresponsivity. The thermoresponsive behavior of hollow microgels differs fundamentally from that of homogeneous systems, as the presence of a cavity enables additional deformation pathways. Upon heating across the VPTT, the collapse of the polymer network does not necessarily occur uniformly, but can involve inward redistribution of polymer chains, partial filling of the cavity, or preservation of the void depending on shell properties. As a result, the thermoresponse reflects a competition between shell elasticity, osmotic pressure, and solvent transport across the network.

Wahrmund et al. [78] investigated the swelling kinetics of hollow PNIPAM microgel shells synthesized using microfluidic devices. Fig. 4A shows the temperature dependence of the inner and outer radii of the hollow microgel shells. Both radii decrease with increasing temperature, indicating thermoresponsive behavior, whereas the volume phase transition temperature is shifted to higher values due to the incorporation of ionic comonomers such as 2-(methacryloyloxy) ethyl trimethyl ammonium chloride (METAC), allylamine. A Comparison with solid microgels highlights that the presence of the cavity introduces additional dynamical features, reflecting the coupling between shell collapse and solvent transport.

Dubbert et al. [84] used small-angle neutron scattering (SANS) to quantify the evolution of cavity size and shell thickness as a function of temperature. Fig. 4B illustrates the swollen and collapsed states of hollow nanogels. Importantly, the cavity size, especially for the soft shell, is often smaller than the original template, indicating inward swelling of the shell into the cavity. The extent of inward collapse of the polymeric shell strongly depends on the crosslinking density: softer shells (low crosslinking) collapse into the cavity at high temperatures (above VPTT), whereas stiffer shells preserve the internal voids. This demonstrates that, unlike conventional microgels, hollow systems undergo complex internal rearrangements rather than a simple homogeneous collapse. Characterization of core–shell and hollow microgels synthesized using different sacrificial templates (e.g., silica or gold) further shows that removal of the core does not significantly affect the VPTT (Fig. 4C), but strongly influences the internal structure [85]. At low temperatures, hollow and core–shell particles exhibit similar sizes, whereas at high temperatures differences emerge depending on shell stiffness. These observations highlight that whether the cavity is preserved or filled at elevated temperatures is governed primarily by shell mechanics and architecture. Importantly, the thermoresponsive behavior of hollow microgels is generally reversible, with repeated swelling and deswelling cycles leading to reproducible changes in size and internal structure. However, the degree of reversibility can depend on the shell architecture and permeability. In systems with highly deformable shells or significant internal restructuring, partial hysteresis or kinetic trapping can occur [28].

Hollow microgels can be engineered to exhibit multi-responsive behavior by constructing concentric shells composed of polymers with distinct transition temperatures, such as PNIPAM and PNIPMAM [57,86,87]. In such systems, each shell undergoes a separate transition, leading to spatially resolved and sequential structural changes. Fig.

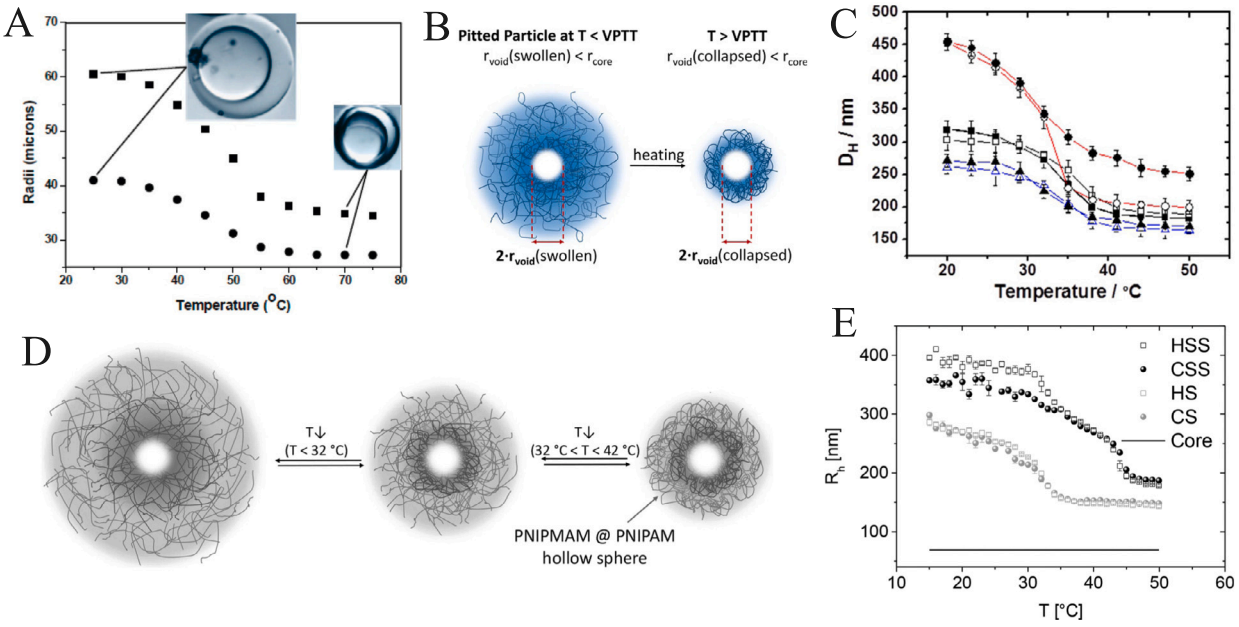

Fig. 4. (A) Inner and outer radii of an ionic hollow microgel shell as a function of temperature. This figure was reproduced with permission from [78]. (B) Schematic representation of a hollow microgel in swollen and collapsed states. This figure was adapted with permission from [84]. (C) Hydrodynamic diameters of Au@pNIPAM particles (filled symbols) and hollow microgels (open symbols) with different crosslinking densities 5% (circle symbols), 10% (square symbols), and 17.5% (triangles) as a function of temperature. Reproduced with permission from Ref. [85]. (D) Depiction of the thermoresponsive behavior of the doubly temperature-responsive hollow microgels. (E) Plot of the hydrodynamic radii of hollow microgels with a single PNIPAM shell (HS, gray symbols) and a PNIPAM/PNIPMAM double shell (HSS, black symbols) *vs.* suspension temperature compared to their parent core–shell (CS) and core–shell–shell (CSS) particles. *Source:* Reproduced with permission from Ref. [57].

4D illustrates this behavior, where the inner and outer shells collapse at different temperatures. Experimental studies have shown that these shells are not independent but interpenetrate at their interface, leading to coupled swelling behavior [88,89]. Consequently, the presence of multiple shells allows for fine control over the internal structure and responsiveness, enabling independent tuning of the inner and outer regions. Fig. 4E shows that hollow microgels with multiple shells exhibit multiple transitions, whereas core removal primarily affects the swollen state, leading to larger particle sizes owing to the inward redistribution of polymer chains. In the context of hollow microgels, most studies report changes in their overall dimensions as a function of temperature (T). However, such a description may not adequately capture the intrinsic swelling behavior. A more appropriate representation of swelling behavior of the hollow microgels could be defined as $S = \frac{R^3(swollen) - R_c^3(swollen)}{R^3(collapsed) - R_c^3(collapsed)}$, where R and R_c are the total radius of the hollow microgel and the radius of the cavity, respectively.

Responsiveness to pH and ionic strength. The introduction of ionizable comonomers further expands the responsiveness of hollow microgels. Copolymerization of PNIPAM with acidic or basic groups introduces sensitivity to pH and ionic strength, enabling control over swelling via electrostatic interactions and osmotic pressure differences.

Wypysek et al. [38,90] demonstrated that hollow microgels containing ionizable dimethyl itaconate (DMI) groups exhibit strong pH-dependent swelling (Fig. 5A–C). At low pH, the network is neutral and thermoresponsive, whereas at high pH the charged network leads to strong swelling driven by electrostatic repulsion and counterion osmotic pressure (Fig. 5(A–B)). Increasing ionic strength reduces the Debye screening length, leading to decreased repulsion and contraction of the microgel (Fig. 5C). Notably, the inner and outer regions of the shell respond differently, reflecting heterogeneities in crosslinking density and internal structure. Similar results were reported by Hazra et al. [28] for much larger hollow microgels for which partial hysteresis or kinetic trapping can occur, particularly when solvent transport across the shell becomes limiting [28,78].

Simulation insights. Simulation studies provide additional insight into the responsive behavior of hollow microgels. Rank et al. [91] demonstrated that hollow microgels exhibit a distinct filling temperature, at which the internal cavity collapses, separate from the intrinsic VPT of the polymer network (Fig. 5D). This indicates that structural reorganization of the cavity and global volume collapse are decoupled processes. Fig. 5E shows that while the overall size change remains continuous, internal density profiles reveal significant restructuring, with polymer chains progressively filling the cavity at high temperatures. The stability of the cavity is strongly influenced by crosslinking density and shell thickness, with stiffer shells preserving the cavity to higher temperatures.

Overall, these results demonstrate that responsiveness in hollow microgels arises from a complex interplay between network elasticity, osmotic pressure, permeability, and confinement. Unlike conventional microgels, hollow systems can exhibit multiple, decoupled structural transitions, making them highly versatile platforms for responsive soft materials.

4. Hollow nano/microgels under stress: Deswelling or buckling?

Conventional cross-linked microgels have been widely used as model systems to explore phase behavior in soft colloidal suspensions, including crystallization, glass transitions, and jamming [93–98]. In crowded environments, where particles are packed beyond random close packing, microgels accommodate external stress through a combination of isotropic deswelling, interpenetration, and structural deformation such as faceting [12,22,99]. In particular, increasing osmotic pressure has been shown to induce progressive deswelling of conventional microgels, reflecting a balance between osmotic forces and network elasticity [100]. The extent of these responses is strongly governed by the microgel softness, which is determined by crosslinking density and internal architecture [22,81]. In contrast to homogeneous

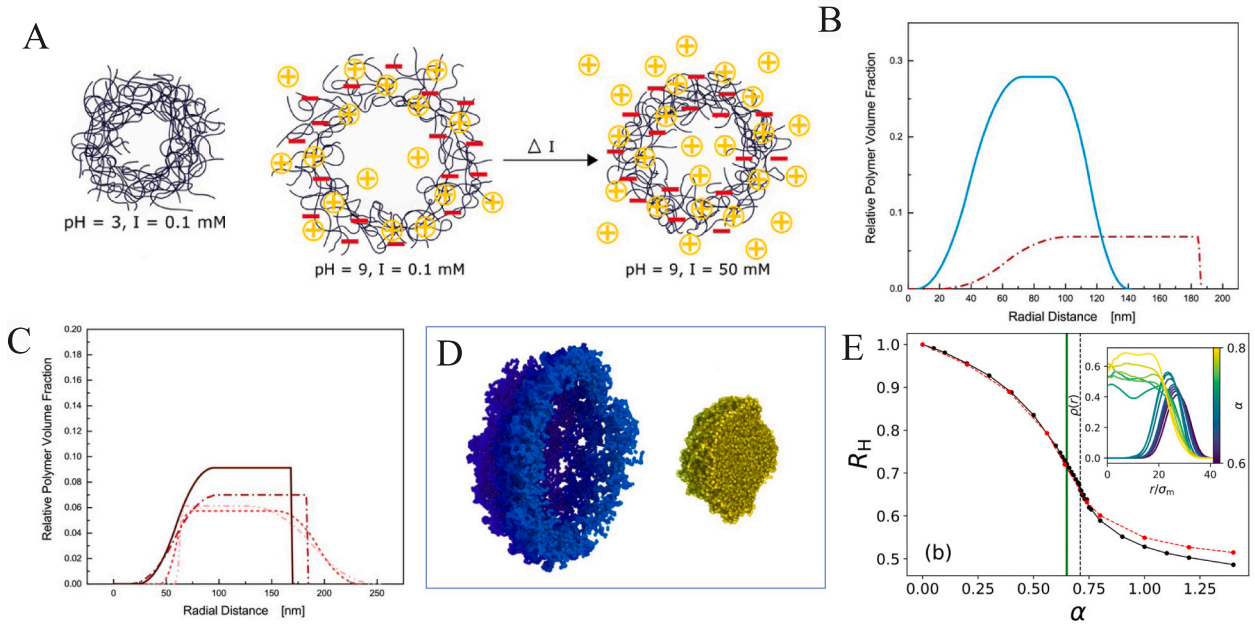

Fig. 5. (A) Schematic representation of anionic hollow microgels at different pHs and ionic strengths. Relative polymer volume fraction of the (B) hollow microgel at pH 3 (blue solid line) and pH 9 (red dashed line) at ionic strength I = 10 mM. (C) Hollow microgel at pH = 9 and at different ionic strengths I = 0.1 mM, I = 1 mM, I = 10 mM, I = 50 mM (light to dark red). Reproduced with permission from Ref. [90]. (D) Simulation snapshot of hollow microgel in swollen (blue) and collapsed (yellow) states. (E) Plot of the hydrodynamic radius of the hollow (black) and non-hollow (red) microgels versus effective temperature, α. The inset shows radial density profiles of the hollow microgel at different temperatures.
Source: Reproduced with permission from Ref. [91].

microgels, compression of hollow systems can be achieved not only through uniform deswelling but also via inward redistribution of the polymer network or mechanical instabilities of the shell, such as buckling.

As a result, hollow microgels provide a unique platform to investigate how internal structure controls the mechanical response of soft colloids under confinement and external pressure. In this section, we examine experimental and simulation approaches used to probe hollow nano/microgels in crowded environments and under applied osmotic stress, with particular emphasis on the competition between deswelling and buckling, and the role of particle size, shell thickness, and crosslinking density in determining the dominant deformation pathway.

Deswelling of hollow microgels in crowded environments and under external pressure. The presence of an internal cavity fundamentally alters the accommodation of external stress by hollow microgels in crowded environments compared to conventional microgels [48,49,81] with an additional deformation pathway arising from the redistribution of polymer chains into the internal cavity. This behavior has been investigated using a combination of scattering techniques and simulations. Fig. 6A shows simulation cross-sections of hollow microgels at increasing degrees of compression (α). At high volume fractions exceeding close packing, the fuzzy shell is progressively compressed due to interactions with neighboring particles, while the overall spherical morphology is largely preserved.

The corresponding radial density profiles (Fig. 6B) reveal that, at high compression, the cavity becomes progressively filled by polymer chains, accompanied by a marked decrease in shell fuzziness. This inward deswelling mechanism allows hollow microgels to accommodate external stress without significant shape distortion. Consequently, these systems can sustain high packing fractions while maintaining their structural integrity. At higher compression levels, simulations further indicated the emergence of faceting, where microgels adopted polyhedral shapes consistent with the surrounding packing geometry (Fig. 6A). Compared to conventional microgels with similar crosslinking densities, hollow systems exhibit a significantly enhanced capacity for deswelling [92]. In particular, hollow microgels have been shown to suppress crystallization over a wide range of conditions [26,49]. This behavior arises from their ability to reduce their effective volume through internal rearrangement. By delaying the onset of excluded-volume constraints, this mechanism hinders the formation of ordered structures and stabilizes disordered phases.

The mechanical response of hollow microgels under external osmotic stress further highlights the importance of their internal architecture. Measurements of particle compressibility using externally applied osmotic pressure, combined with scattering techniques (Fig. 6C), revealed a continuous decrease in particle size with increasing pressure [92]. Hollow nanogels with larger cavities (HN1 in Fig. 6C) exhibited significantly greater compression at lower osmotic pressures, indicating enhanced softness, whereas particles with smaller cavities (HN2 in Fig. 6C) required substantially higher pressures to achieve comparable deswelling. These findings demonstrate the strong influence of cavity size on the mechanical properties and compressibility of hollow microgels.

Buckling of hollow microgels under external stresses. In contrast to nanoscale hollow microgels, which were found to primarily accommodate stress through inward deswelling, microscale hollow microgels exhibit a qualitatively different mechanical response dominated by shell instabilities. The presence of a large internal cavity, combined with a thin elastic network, enables buckling as an additional pathway for stress relaxation under external pressure. The onset of such instabilities is strongly governed by the ratio between cavity size and shell thickness, with thin shells surrounding large cavities being particularly prone to buckling [51].

This behavior has been investigated using hollow microgel capsules with micrometer-sized cavities [28,51]. The larger length scale allow direct in situ observation using optical and confocal microscopy, as well as light scattering techniques. A schematic representation of the particle geometry, characterized by the shell radius R_S and thickness δ, is shown in Fig. 7A. External osmotic pressure was applied using polymer solutions of PEG and dextran, employed as osmolytes with

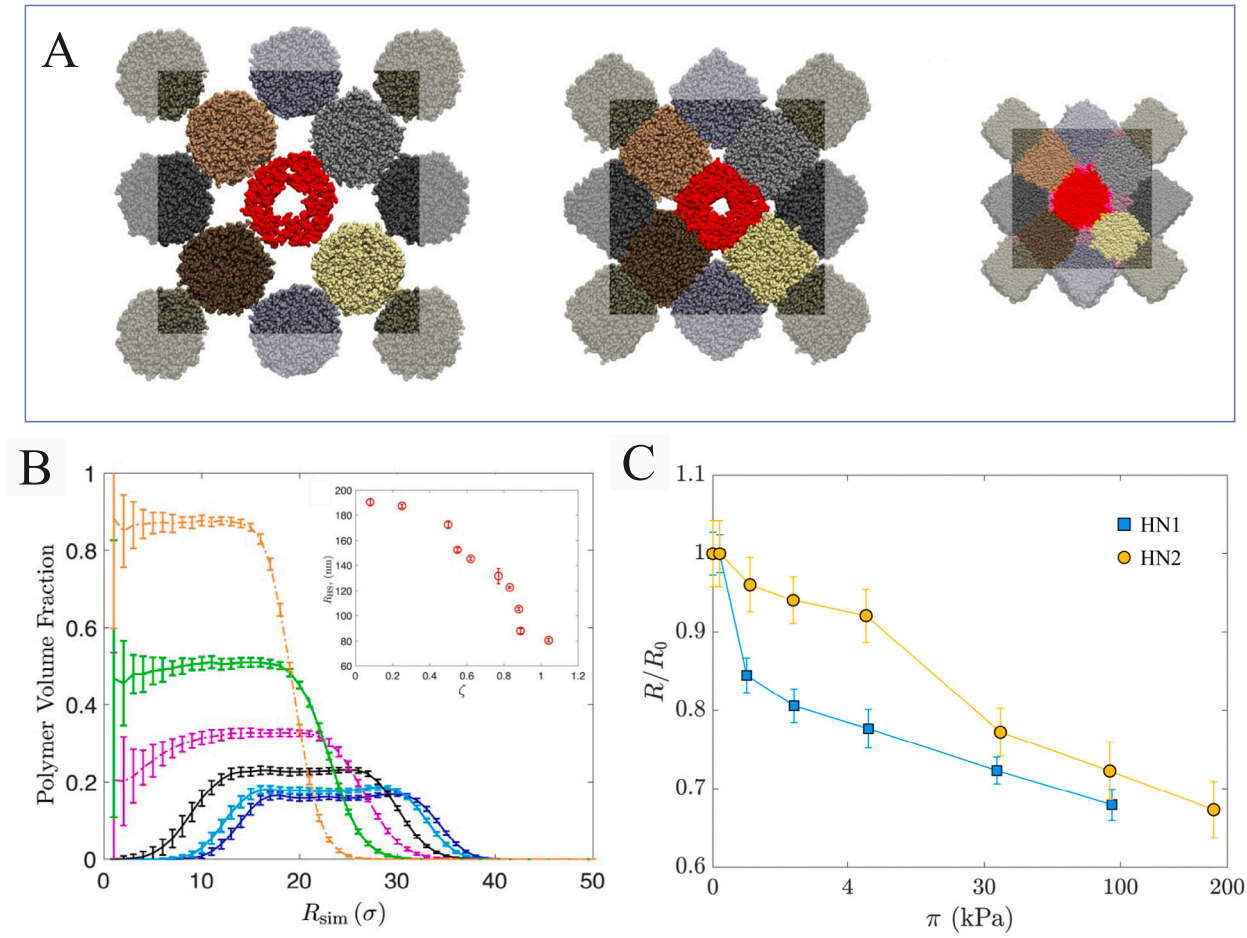

Fig. 6. (A) Cross section of the simulation box through the center of mass of the hollow microgel (red) at different compression degrees α: α = 1, 0.8, and 0.5 from left to right, respectively. (B) Polymer volume fraction as obtained from the computer simulations in the hollow microgels as a function of radial coordinate R_{sim} at different degrees of compression α (α = 1, 0.9, 0.8, 0.7, 0.6, and 0.5), with the curves progressing from dark blue for α =1 to orange for α = 0.5. The inset shows the radius of the hollow microgels as a function of the generalized volume fraction (ζ) measured using SANS. These figures were adapted with permission from Ref. [48]. (C) Dependence of the normalized radius, R/R_0, on the suspension osmotic pressure, π, for hollow microgels with two different cavity sizes. The radius R_0 corresponds to the particle radius in the absence of externally applied osmotic pressure (π = 0).
Source: Adapted with permission from Ref. [92].

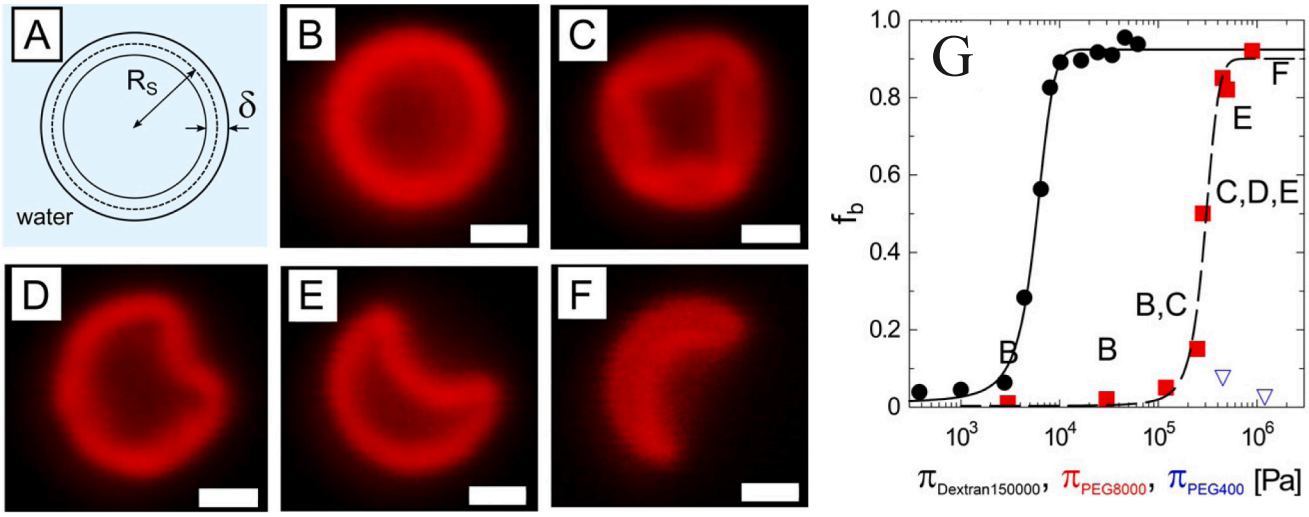

Fig. 7. (A) Schematic of the hollow microgels. (B–F) Confocal micrographs of the hollow microgels, highlighting the typical configurations observed upon increasing the osmotic pressure by adding PEG 8000. Scale bars indicate 500 nm. (G) Fraction of buckled microgel capsules as a function of the osmotic pressure observed by adding PEG 400 (triangles), dextran 150 000 (circles), and PEG 8000 (squares).
Source: Reproduced with permission from Ref. [51].

varying molecular weights corresponding to known osmotic pressures. A key observation is that buckling occurs when the external osmotic agent cannot penetrate the shell efficiently. Short polymers, such as PEG 400, diffuse into the particles, equilibrating the osmotic pressure and preventing deformation. In contrast, larger polymers (e.g., dextran 150 000) remain excluded and do not diffuse through the shell, generating an effective pressure difference across the shell and triggering buckling at relatively low osmotic pressures. As the applied pressure increases, the microgel particles exhibit a sequence of distinct deformation modes (Fig. 7B–F). At low pressures, particles remain spherical. With increasing stress, localized indentations appear, ranging from small dimples to multiple depressions per particle. Above a critical buckling pressure, a transition to concave, bowl-like shapes is observed, followed at higher pressures by nearly complete collapse of the shell.

The role of osmolyte permeability is further quantified in Fig. 7G, which shows the fraction of buckled microgels (f_b) as a function of the applied osmotic pressure for PEG 400, PEG 8000, and dextran 150 000. For PEG 400, which can readily permeate the microgel shell, little or no buckling is observed because the osmotic pressure equilibrates across the shell. In contrast, the larger PEG 8000 and dextran 150 000 molecules are more effectively excluded from the microgel interior, allowing a pressure difference to develop across the shell and producing a progressive increase in the fraction of buckled particles with increasing osmotic pressure.

This behavior can be quantitatively described within the framework of classical thin-shell elasticity as it was done for instance for polymer capsules [101,102]. The critical buckling pressure is given by

$$p_c = \frac{2E\delta}{3(1-\nu^2)R_s^2}, \tag{1}$$

where E and ν are the Young's modulus and Poisson's ratio, respectively. The experimental data are well captured by this model, indicating that hollow microgels at this scale behave as soft elastic shells. Importantly, the deformation is reversible, with particles recovering their initial spherical shape upon removal of the osmotic stress, highlighting their robustness and potential for repeated actuation [51]. The results of this study were further supported by computer simulations.

A similar buckling response has been observed in ultrathin hydrogel shells produced via layer-by-layer assembly [103]. Under increasing osmotic pressure, these systems undergo a sharp transition from spherical to concave morphologies once a critical stress is reached (Fig. 8A–D). The transition occurs in a highly cooperative manner across the population, reflecting the shells' structural homogeneity. Fig. 8E shows that the buckling of the spherical hydrogel shells occurs above a critical osmotic pressure that increases with the shell thickness. The fraction of buckled particles increases sigmoidally with increasing poly(styrene sulfonate) (PSS) concentration, with thinner shells buckling at lower osmotic pressures. The critical pressure scales with shell thickness according to classical shell theory Fig. 8F, confirming that the mechanical response is governed primarily by geometry. Notably, the deformation is fully reversible and occurs on short timescales, emphasizing the importance of shell permeability and rapid solvent transport.

Beyond isolated particles, the mechanical response of hollow microgels is further enriched in dense suspensions. In mixtures of hollow and conventional microgels, the presence of hollow particles significantly modifies interparticle interactions and phase behavior [26]. Simulations of the potential of mean force (Fig. 9A) show that interactions involving hollow microgels are softer and more favorable under compression, as deformation is primarily accommodated by the hollow particle. This enhanced deformability increases the configurational entropy of the system and suppresses crystallization at high concentrations. A recent study further demonstrated that the effective interactions between hollow microgels can be described remarkably well by a Hertzian potential. In particular, an effective Hertzian-fluid representation reproduces the static radial distribution functions of the fully resolved hollow-microgel system over an extended range of

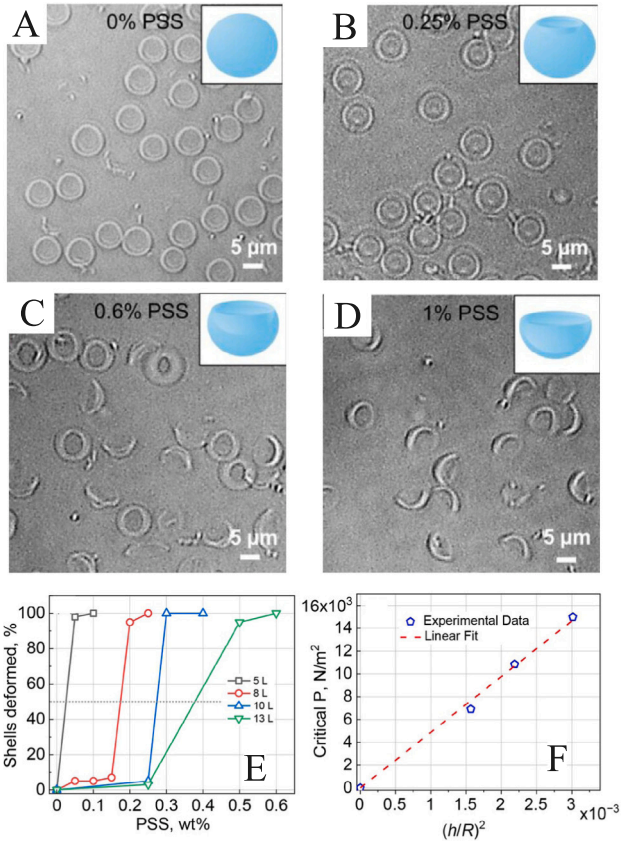

Fig. 8. Optical microscopy images of spherical (P(MAA)13 multilayer hydrogel shells in buffer solution at pH 7 in the presence of poly(styrene sulfonate) (PSS) polymer chains at concentrations of (A) 0 wt%, (B) 0.25 wt%, (C) 0.6 wt%, and D) 1 wt% with the insets schematically depicting capsule deformation. (E) Shell deformation in % of multilayer hydrogel with varying thicknesses as a function of PSS concentration. (F) Plot of critical bucking pressure *vs.* $(h/R)^2$, where h (or δ) and R are the shell thickness and radius of hydrogel capsules.
Source: Reproduced with permission from Ref. [103].

packing fractions well beyond particle overlap. This behavior contrasts with conventional microgels, for which pairwise effective descriptions typically lose accuracy in highly crowded states as internal deformation and many-body contributions become increasingly important. However, their internal degrees of freedom lead to faster dynamics and deviations from simple models, especially near the glass transition, highlighting the complexity of their collective behavior [104]. Buckling and strongly anisotropic deformation of hollow microgels can also occur without external osmotic compression. In mesoscopic simulations, Anakhov et al. [105] studied hollow microgels in highly asymmetric mixtures of two immiscible liquids. Preferential absorption of the minor component into the polymer shell or cavity caused major internal redistribution and, under suitable solvent conditions, induced anisotropic particle shapes. This showed that cavity-mediated deformation can be triggered by selective solvent uptake. Recent simulations demonstrate that, at sufficiently high packing fractions, hollow microgels undergo spontaneous anisotropic deformations driven purely by crowding [50]. As shown in Fig. 9B, particles develop inward dents and irregular shapes, indicating localized shell collapse. The degree of deformation depends on the local packing environment, with close contacts inducing inward buckling of the shell.

Analysis of the pair correlation function and local structure (Fig. 9C–G) reveals that short-range contacts play a crucial role in initiating deformation. At intermediate densities, isolated contacts lead to localized distortions, whereas at higher packing fractions multiple neighbors

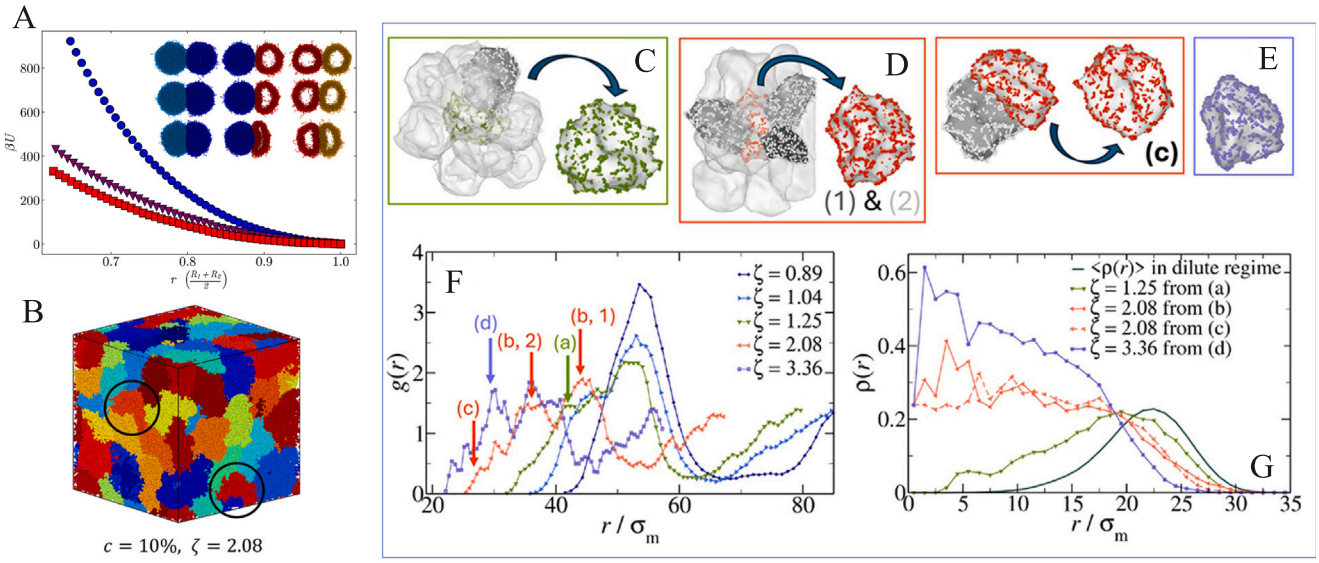

Fig. 9. (A) Potential of mean force (PMF) as a function of the relative particle distance for different microgel interactions. The blue circles, purple triangles, and red squares represent two regular microgels, regular and hollow microgels, and two hollow microgels, respectively. The simulation snapshots display a central slice of the deformed microgels for all different pairs of microgels at three distances (from top to bottom $r = 0.95$, 0.85, 0.70. Adapted with permission from Ref. [26]. (B) Simulation snapshot of hollow microgel with crosslinker concentration, c = 10% and at packing fraction, $\zeta = 2.08$. Snapshots of nearest-neighbor hollow microgels with c = 10% at separations corresponding to the peaks in the radial distribution function. The peaks are indicated by color-coded arrows in panel (F). The central microgels are highlighted as: (C) green at ~42 σm ($\zeta = 1.25$); (b) red at ~44 σm (labeled 1) and ~35 σm (labeled 2) for $\zeta = 2.08$; (c) red at ~28 σm; and (d) violet at $\zeta = 3.36$, showing no further deformation at high density. (F) Radial distribution functions g(r) at different packing fractions, with color-coded arrows identifying the nearest-neighbor configurations shown in panels C–E. (G) Radial monomer density profiles of the corresponding color-highlighted microgels at the configurations shown in panels C–E, compared with the average radial monomer density profile of hollow microgels in the dilute regime. The progressive accumulation of monomers toward the particle center illustrates filling and eventual collapse of the internal cavity upon deformation.
Source: Reproduced with permission from Ref. [50].

induce complex, multi-dimpled shapes. In this regime, the hollow cavity progressively collapses as polymer material is redistributed inward, and the particles lose their initial spherical symmetry. These results demonstrate that, in dense dispersions, buckling can be a collective phenomenon arising from many-body interactions rather than externally imposed pressure gradients. The mechanical response is therefore governed by the interplay between shell elasticity, particle architecture, and local packing constraints. In this context, hollow microgels occupy an intermediate position between classical soft colloids and elastic capsules. While the term "capsule" remains somewhat controversial for these systems, it nonetheless reflects their ability to sustain stresses and undergo shell-like mechanical instabilities characteristic of thin elastic membranes.

In summary, hollow microgels exhibit two distinct regimes of mechanical response under stress. At small length scales, deformation is dominated by inward deswelling and progressive filling of the cavity, leading to enhanced compressibility. At larger length scales, where the shell becomes thin relative to the cavity size, the mechanical response is governed by elastic instabilities, and buckling emerges as the dominant mode of deformation. This highlights the central role of the core-to-shell size ratio, together with the shell elasticity determined by the crosslinking density, in determining whether a hollow microgel undergoes smooth deswelling or abrupt shape transformations. Although osmotic-pressure-induced buckling has been experimentally demonstrated, achieving controlled and reversible buckling in response to external stimuli remains largely unexplored. In this context, hollow microgels offer a unique opportunity to design shape-shifting colloids by exploiting the softening of the polymer network close to the volume phase transition temperature (VPTT). In principle, coupling this intrinsic thermoresponsivity with an externally tunable osmotic pressure could enable reversible transitions between spherical and buckled states.

A key parameter in this perspective is the permeability of the shell, which governs the buildup of osmotic pressure across the microgel. Controlling solute transport through the shell by tuning mesh size, crosslinking density, or polymer–solute interactions provides a direct route to regulate the onset of buckling. In this regard, multiresponsive hollow microgels incorporating charged or functional comonomers offer additional degrees of control, as their permeability and internal osmotic balance can be modulated via pH, ionic strength, or temperature.

It is important to note that further development of experimental methodologies is needed to accurately characterize hollow microgels, particularly for reliable quantification of cavity volume, which would benefit from the use of super-resolution imaging techniques combined with robust analytical approaches. In addition, a systematic investigation of the buckling behavior of hollow microgels as a function of particle size, crosslinking density, shell thickness, and shell-to-core ratio would provide valuable insights and is an important direction for future research. These systems would not only provide new insight into the mechanics of soft shells under external stresses, but also open avenues toward stimuli-responsive shape morphing materials and soft micromechanical actuators. Moreover, the thermally induced shape fluctuations reported by Hazra et al. [28] underscore the need for a systematic investigation of such dynamics, as they provide a direct means to quantify the bending rigidity of large hollow microgels.

5. Interfacial assembly: Spreading or No spread?

Both conventional and hollow microgels strongly adsorb to liquid/liquid and air/water interfaces owing to the significant reduction in interfacial tension [3,12]. Similar to hard colloids, microgels can stabilize Pickering emulsions and form densely packed monolayers at fluid interfaces [106–108]. However, in contrast to rigid particles, their internal polymer network allows for deformation and partial spreading upon adsorption, enabling a reduction in interfacial energy.

For conventional microgels, this deformation is governed by a balance between interfacial tension and network elasticity, which can

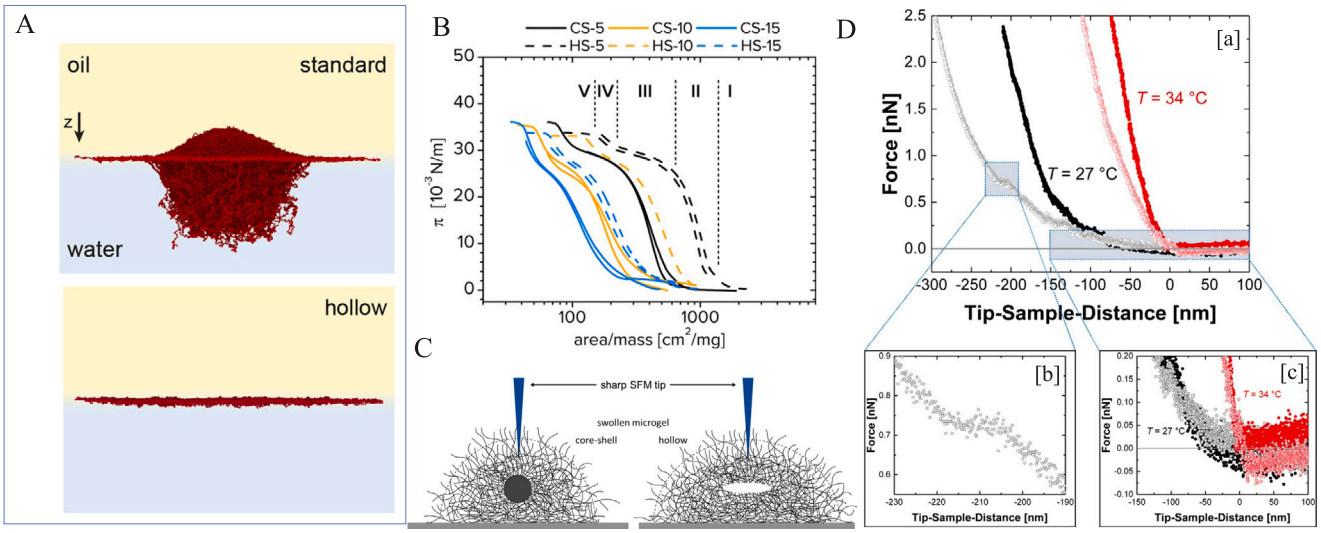

Fig. 10. (A) Snapshots of conventional and hollow microgel adsorbed on water (blue)/oil (yellow) interface. Reproduced with permission from Ref. [53]. (B) Surface pressure as a function of relative area. Solid lines: core–shell particles (CS). Dashed lines: hollow microgel (HS). Black: CS/HS-5; orange: CS/HS-10; blue: CS/HS-15, where 5, 10, and 15 denote the nominal crosslinker concentrations in mol%. Reproduced with permission from Ref. [52]. (C). Schematic illustration of a sharp tip approaching the water/microgel interface, probing the density variation near the tip for a swollen core–shell microgel (left) and a hollow microgel (right). (D) Force–distance curves of a core–shell microgel (CS, filled circles) and hollow microgel (HS, open circles) at $T = 27°C$ (CS: black, HS: light gray) and $T = 34°C$ (CS: red, HS: light red); (a) total force scale; (b) magnified graph of the kink within a range of tip-sample distances between 205 and 215 nm. (c) Magnified graph of the lower-force region.
Source: Reproduced with permission from Ref. [82].

be tuned via crosslinking density and internal architecture. Hollow microgels introduce an additional level of complexity, as the presence of a solvent-filled cavity enhances their effective softness by enabling internal polymer redistribution. As a result, hollow microgels generally exhibit stronger deformation and flattening at interfaces compared to conventional or core–shell systems. This difference is illustrated in Fig. 10A, where simulations show a more pronounced spreading of hollow microgels at the oil/water interface. Despite this enhanced deformability, hollow microgels do not necessarily undergo complete spreading. This behavior is reminiscent of the mechanical response discussed in the previous section, where internal architecture limits the extent of deformation despite enhanced softness. Instead, their interfacial configuration reflects a competition between interfacial tension and the elastic resistance of the shell. This raises a central question: to what extent can hollow microgels spread, and which parameters control this behavior?

Compression isotherms provide direct insights into this balance. Measurements of surface pressure as a function of interfacial area (Fig. 10B) reveal a two-stage response, corresponding to different regimes of particle interaction and deformation [52]. Hollow microgels exhibit an earlier increase in surface pressure compared to core–shell systems, indicating a larger effective footprint and enhanced spreading at low compression. This effect is further amplified at low crosslinking densities, where reduced shell stiffness promotes deformation. At higher compression, however, the response diverges: while core–shell microgels display a steep increase in surface pressure due to the presence of a rigid core, hollow microgels remain more compliant, reflecting their ability to redistribute polymer within the shell. The role of internal structure becomes even more apparent when probing microgels adsorbed on solid substrates. Force spectroscopy measurements using scanning force microscopy (Fig. 10C–D) show that hollow microgels exhibit deeper indentation compared to core–shell systems, confirming their increased deformability [82]. Interestingly, despite significant compression upon adsorption, the cavity is not entirely eliminated (Fig. 10C). Instead, it persists in a reduced form, indicating that interfacial confinement leads to deformation rather than complete collapse. This observation highlights that the internal architecture continues to play a role even under strong confinement.

Direct visualization of hollow microgels at liquid interfaces further confirms their pronounced but finite deformation. Confocal microscopy studies of micron-sized hollow microgel capsules (Fig. 11A–B) show that particles flatten upon adsorption, with the degree of deformation depending strongly on the interfacial tension [51]. The contact radius, a, increases with increasing surface tension difference, consistent with a balance between adhesion energy and shell elasticity (Fig. 11C–D). This behavior could be quantitatively described using an extension of the Johnson–Kendall–Roberts (JKR) [109,110] framework for soft elastic shells,

$$a \approx \left(\frac{W R_s^4 (1-\nu^2)}{E\delta^2} \right)^{1/3}, \tag{2}$$

where W is the interfacial energy and E, ν, and δ denote the Young's modulus, Poisson ratio, and shell thickness. While this approach captures the observed trends, JKR theory is formally derived for elastic solids in contact with rigid substrates and assumes localized deformation. Its application to microgels at fluid interfaces, where deformation is often large and spatially distributed, should therefore be interpreted with caution.

Interestingly, the interfacial energy extracted from the shell model (Eq. (2)) was found to scale linearly with $\Delta\gamma$, defined as the difference in surface tension between the bare interface and the interface saturated with smaller microgels, as independently determined by pendant-drop measurements (Fig. 11D). This observation suggests that the effective driving force for deformation is directly related to the reduction of interfacial tension induced by microgel adsorption. In this context, the quantity W should be interpreted as an effective adhesion or interfacial energy, rather than a well-defined thermodynamic surface energy as in the case of rigid particles. For microgels, which consist of a deformable and permeable polymer network, the notion of a sharp interface is inherently ambiguous, as polymer chains can extend and spread within the interfacial region. Consequently, the interfacial energy cannot be uniquely defined at the particle level and is more appropriately related to the macroscopic change in interfacial tension upon adsorption. The proportionality between W and $\Delta\gamma$ observed in Fig. 11C–D, therefore, provides a practical way to link microscopic deformation to macroscopic interfacial properties.

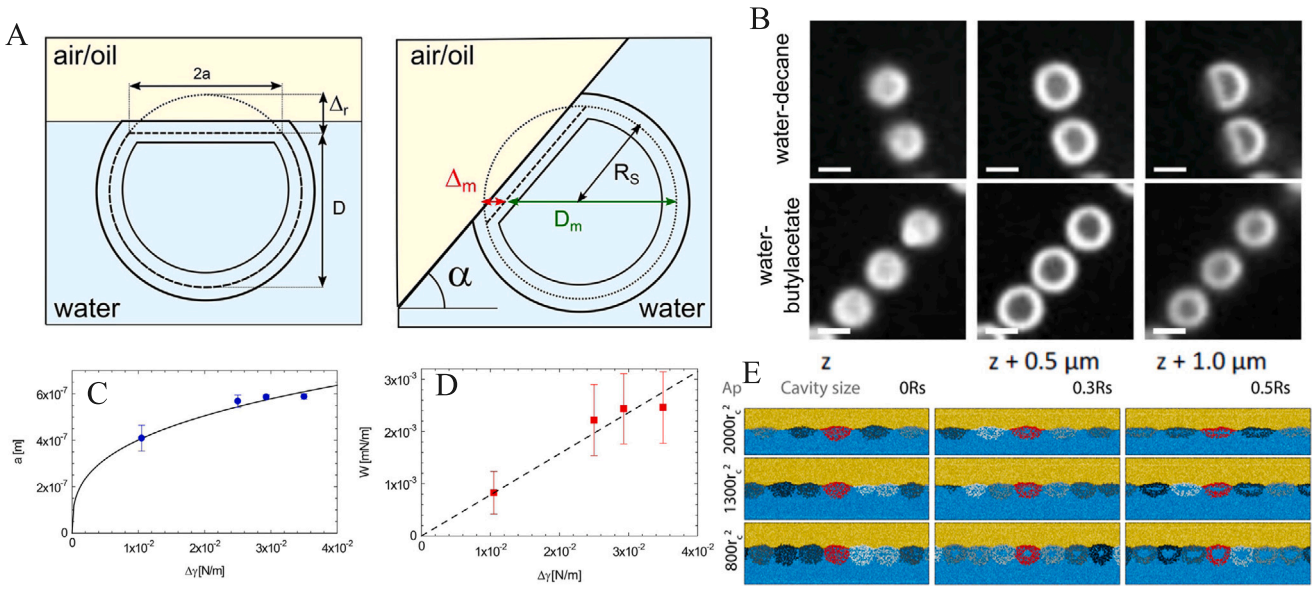

Fig. 11. (A) Schematic representations of the hollow microgels adsorbed at flat (left) or tilted (right) air/oil–water interfaces. (B) Hollow microgels imaged at different interfaces with a 0.5 μm increment in z. Scale bars: 1 μm. (C) Contact radius as a function of surface tension differences ($\Delta\gamma$). The solid line is fitted to the shell model Eq. (2). (D) Plot of estimated interfacial energy, W, $vs.$ $\Delta\gamma$. The data were fitted with a straight line passing through the origin. These figures were adopted from Ref. [51]. (E) Side views of the simulation of hollow microgel monolayers at the water/oil interface with different cavity sizes and compression degrees.
Source: Reproduced with permission from Ref. [111].

This distinction also highlights a key difference between microgels at fluid interfaces and soft particles on solid substrates. At fluid interfaces, the relevant driving force is governed by interfacial tension, which is typically orders of magnitude larger than adhesion energies encountered in solid contacts. Consequently, capillary forces can dominate over elastic resistance, leading to significantly enhanced deformation. At the same time, the soft and adaptive nature of the microgel interface prevents a direct mapping onto classical contact mechanics frameworks, reinforcing the need for scaling approaches that explicitly account for interfacial tension, elasticity, and internal structure.

In contrast, microgels at fluid interfaces typically experience larger and more distributed deformations, such that the assumptions of localized contact underlying Hertzian or JKR descriptions no longer strictly apply. A useful framework to rationalize this regime is provided by elastocapillarity, as developed for soft solids by Style, Dufresne and co-workers [112,113]. In this approach, deformation is governed by the competition between interfacial tension and bulk elasticity, which introduces an intrinsic length scale, the elastocapillary length $\ell_{ec} \sim \gamma/E$, where γ is the relevant fluid–fluid interfacial tension. When the particle size becomes comparable to or smaller than this length scale, interfacial stresses are sufficient to induce significant deformation of the entire object. In this regime, deformation is no longer confined to a localized contact zone, but instead involves a global reshaping of the particle. For microgels, where R is often comparable to ℓ_{ec}, this condition is readily fulfilled, explaining their pronounced deformation at fluid interfaces.

Extending this framework to hollow microgels, elasticity is no longer only governed by bulk deformation of the particle, but also by bending and stretching of the shell. As reflected by the scaling introduced in Eq. (2), this leads to a stronger dependence of the contact radius on particle size ($a \sim R_s^{4/3}$) compared to bulk microgels ($a \sim R^{2/3}$), and highlights the key role of the hollowness parameter δ/R_s. From a mechanical perspective, this behavior can be rationalized using classical thin shell theory [114,115], as well as more recent developments in soft matter and elastic shells [116,117], where deformation arises from a competition between stretching and bending modes. The stretching energy scales as $E_{str} \sim E\delta\epsilon^2 R^2$, where ϵ denotes the characteristic in-plane strain of the shell, while the bending rigidity scales as $\kappa \sim E\delta^3$. As a result, sufficiently thick shells primarily resist deformation through stretching, whereas thinner shells can more easily accommodate deformation through bending. This reduction in effective stiffness with decreasing shell thickness is consistent with the scaling $a \sim (WR^4/(E\delta^2))^{1/3}$ derived for adhesive elastic shells [110], and explains the enhanced spreading observed in hollow microgels. Such approach based on energy balance for thin elastic shells corresponds to a regime of larger, global deformation dominated by stretching of the shell [110].

In this framework, varying the ratio δ/R_s provides a continuous transition between bulk-like microgels, where elasticity is dominated by volumetric deformation, and thin elastic shells, where bending and in-plane stretching govern the mechanical response. Hollow microgels thus occupy an intermediate regime between bulk elastic particles and fluid droplets, where interfacial deformation is governed by a coupled interplay between capillarity, elasticity, and geometry.

It should be noted that this scaling is derived within the framework of shell mechanics, which assumes small elastic strains despite allowing for large geometric deformation with contact radii comparable to the particle size. As such, it captures regimes of global deformation but does not account for strongly nonlinear responses, such as large strain, plastic rearrangements, or instabilities that may arise at very large deformation, which remain among the main limitations of current theoretical descriptions [112,113]. These limitations highlight that current theoretical descriptions, while capturing key scaling behaviors, do not fully account for the complex, multiscale nature of microgels at fluid interfaces. In particular, they neglect the internal heterogeneity of the polymer network, solvent permeability, and the coupled deformation of both the particle and the interface. In this context, computer simulations provide a powerful complementary approach, as they can explicitly resolve internal structure, polymer redistribution, and interfacial interactions beyond the assumptions of continuum models.

Simulation studies provide further insight into the role of cavity size and compression. Hollow microgels consistently exhibit stronger deformation and flattening compared to conventional microgels, with the

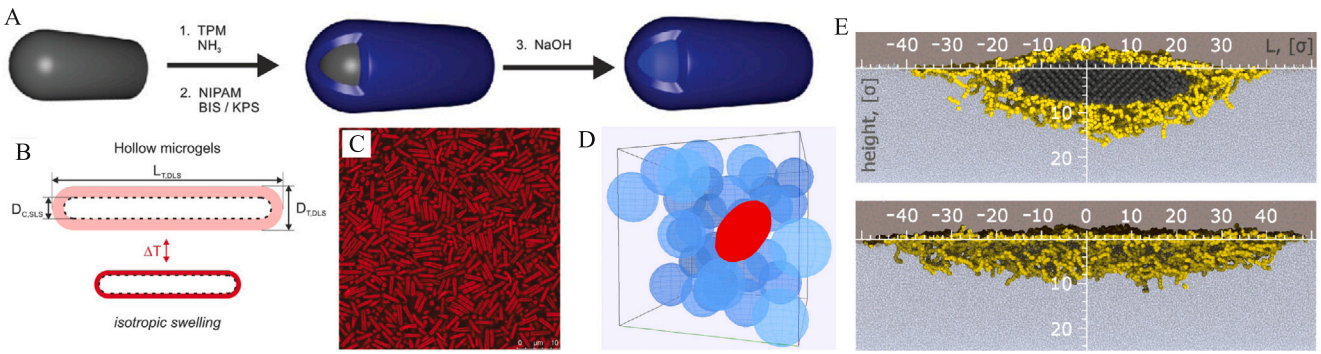

Fig. 12. (A) Schematic illustration of the synthesis procedure to synthesize hollow microgels using silica rods as sacrificial templates. (B) Schematic illustration of the change in the different dimensions of the rod-shaped hollow microgels upon increasing the temperature from 20 to 40°C. (C) Confocal microscopy micrographs of a concentrated suspension of hollow rod-shaped microgels. Reproduced with permission from Ref. [56]. (D) Simulation snapshot, showing one hollow ellipsoidal nanogel (red particle), immersed in a crowded environment of spherical nanogels (blue particles). Reproduced with permission from Ref. [118]. (E) Longitudinal cross-sections of core–shell (upper image) and hollow (lower image) anisotropic microgels at the decane–water interface.
Source: Reproduced with permission from Ref. [54].

effect becoming more pronounced for larger cavities (Fig. 11E) [111]. Under compression, both types of microgels increasingly protrude into the better solvent phase, while hollow microgels additionally undergo changes in cavity shape and partial filling. This indicates that the internal cavity acts as a reservoir for polymer redistribution, enhancing adaptability under interfacial confinement. Recent simulations of amphiphilic hollow microgels at liquid–liquid interfaces further reveal that the cavity itself can exhibit dynamic behavior. Kudryashova et al. [119] showed that the interfacial morphology and cavity integrity are controlled by a competition between liquid–liquid interfacial tension, solvent selectivity toward the different network segments, segment–segment incompatibility, and cavity size. Interestingly, close to the transition between stable hollow and collapsed states, a condition was discovered where the internal cavity cyclically collapsed and reformed. These 'pulsating' states illustrate that interfacial confinement can lead to both static deformation and dynamic restructuring of the hollow structure over time.

In summary, hollow microgels exhibit enhanced but not unlimited spreading at interfaces. Their interfacial behavior is governed by a subtle balance between interfacial tension, shell elasticity, and internal architecture. While the presence of a cavity enhances deformability and promotes spreading, the finite stiffness of the shell and geometrical constraints prevent complete flattening. Therefore, hollow microgels occupy an intermediate regime between soft polymer networks and elastic shells, offering unique opportunities to tailor interfacial properties. Controlling parameters such as cavity size, crosslinking density, and responsiveness opens new avenues for designing adaptive emulsions, responsive coatings, and reconfigurable interfacial materials.

6. Influence of shape anisotropy

While spherical microgels have been extensively studied, the exploration of anisotropic microgels—and in particular hollow anisotropic systems—remains comparatively limited. This is somewhat surprising, as anisotropy introduces additional degrees of freedom, including directionality, curvature-dependent interactions, and orientation-dependent mechanical response, which are absent in isotropic systems [120–123]. In hard colloidal systems, such as silica rods, these features give rise to rich phase behavior, including liquid crystalline ordering and anisotropic self-assembly [124,125]. However, such systems are often limited by sedimentation and kinetic arrest at high volume fractions.

Soft colloids such as microgels offer an attractive alternative, as their size, shape, and mechanical properties can be tuned via external stimuli [12,22]. In this context, introducing both anisotropy and a hollow architecture leads to a unique class of particles in which shape, internal structure, and deformability are intrinsically coupled. These unique characteristics of the anisotropic hollow microgels open new avenues for tailoring the structure, mechanics, and responsiveness of soft matter systems.

Synthesis and design strategies. Recent advances have enabled the fabrication of anisotropic hollow microgels with controlled geometry. In particular, rod-shaped hollow PNIPAM microgels have been synthesized using anisotropic silica templates [56]. As illustrated in Fig. 12A, the synthesis involves (i) preparation of monodisperse silica rods, (ii) surface functionalization with polymerizable groups, (iii) growth of a crosslinked PNIPAM shell, and (iv) removal of the core via etching. This templating strategy allows precise control over particle dimensions and shell thickness, although slight shape evolution of the template during processing can occur due to differential silica condensation [126]. Beyond templating, alternative routes such as uniaxial stretching of microgels [127–129], microfluidic approaches [130], projection photolithography [131], and PRINT techniques [132–134] have also been employed. However, these methods often produce relatively large particles, suffer from low yields, or result in systems with limited Brownian dynamics due to sedimentation.

Stimuli-responsive behavior. Anisotropic hollow microgels retain the characteristic responsiveness of their spherical counterparts, while introducing additional complexity associated with shape. Experimental studies using SLS, DLS, SANS, SAXS, and confocal microscopy have shown that rod-shaped and ellipsoidal hollow microgels undergo thermoresponsive swelling and deswelling across the VPTT (Fig. 12B) [56,135,136]. Interestingly, many systems exhibit nearly isotropic swelling at the particle level, maintaining their overall shape while uniformly changing dimensions. As a result, both particle volume and aspect ratio can be tuned via temperature. However, the internal structure evolves non-trivially: the cavity size and shell thickness respond differently depending on crosslinking density and geometry. For instance, thinner shells promote stronger internal redistribution, while thicker shells preserve cavity integrity even in the collapsed state. In ellipsoidal systems, removal of the core can induce structural transformations, such as transitions from ellipsoidal core–shell particles to cylindrical hollow microgels [135]. These observations highlight that, as in spherical systems, the interplay between shell elasticity and cavity geometry governs the final structure, but here with an additional dependence on curvature and orientation.

Behavior in crowded environments. The coupling between anisotropy and softness becomes particularly evident in dense suspensions. Confocal microscopy of rod-shaped hollow microgels (Fig. 12C) reveals dynamically arrested states with local nematic ordering but no long-range positional order [56]. The ability to tune particle volume

via temperature enables reversible transitions between arrested and fluidized states.

More generally, anisotropic hollow microgels exhibit remarkable adaptability under crowding. Simulations and scattering experiments (Fig. 12D) show that particle shape evolves depending on the surrounding environment [118]. When embedded in a matrix of spherical particles, ellipsoidal hollow microgels tend to reduce their aspect ratio and become more isotropic. In contrast, in anisotropic environments, their elongation is preserved or even enhanced. This behavior reflects a balance between elastic deformation and excluded-volume interactions, and can be interpreted as a form of collective shape adaptation. In this sense, anisotropic hollow microgels behave as "self-adjusting" particles, whose shape is not fixed but determined by their environment.

Interfacial behavior and anisotropic assembly. At fluid interfaces, anisotropic hollow microgels exhibit even richer behavior due to the interplay between shape, curvature, and interfacial forces. Simulations (Fig. 12E) show that hollow anisotropic microgels deform more strongly than their core–shell counterparts, consistent with observations for spherical systems [54]. However, deformation is highly anisotropic, with different responses along the longitudinal and lateral directions. The relative shell thickness and cavity dimensions play a central role: thinner shells and larger cavities promote enhanced elongation and spreading, while thicker shells limit deformation. As a result, the interfacial configuration depends not only on softness but also on particle geometry and local curvature.

The interfacial behavior of micron-sized rod-shaped hollow microgels was also investigated by Hagemans et al. [56]. Hollow rod-shaped microgels spontaneously adsorb and self-assemble at the air–water interface. At low surface coverage, they assemble into long arrays of rods lying side by side owing to capillary interactions [137]. The core–shell microgels also showed side-to-side assembly but appeared less surface-active and did not exhibit long-range ordering. The authors also used hollow rod-like microgels as stabilizing agents for decane emulsion droplets to form Pickering emulsions. Confocal microscopy revealed their dense packing at the interface, primarily along the interface, and their ability to bend and adapt to the local curvature of the droplets, as also reported by Nickel et al. [54] for hollow anisotropic nanogels.

Overall, anisotropic hollow microgels represent a promising yet still underexplored class of soft colloids. By combining shape anisotropy with internal cavities and stimuli-responsiveness, these systems enable coupling between geometry, mechanics, and interactions across multiple length scales. Their ability to adapt shape in response to environmental constraints, exhibit directional interactions, and respond to external stimuli makes them attractive model systems for studying anisotropic soft matter, as well as for applications in responsive emulsions, adaptive materials, and bioinspired systems. Future work should focus on developing scalable synthesis routes, improving control over internal architecture, and exploring the interplay between anisotropy, responsiveness, and collective behavior.

7. Potential applications of hollow microgels

Hollow microgels have attracted increasing attention across a wide range of applications, including biomedicine, interfacial science, and functional materials, owing to their tunable internal architecture, stimuli-responsiveness, and enhanced deformability [139–141]. In particular, the presence of an internal cavity introduces functionalities that are not accessible in conventional microgels, such as the decoupling between storage volume and network elasticity. However, this additional degree of freedom also introduces new constraints, most notably the presence of a permeable shell acting as a transport barrier. As a result, the relevance of hollow microgels for a given application is not universal, but depends on a subtle balance between accessibility, confinement, and controlled release. In the following, we discuss these aspects with a focus on encapsulation and drug delivery.

Encapsulation and drug delivery. Hollow microgels are natural candidates for encapsulation, as their internal cavity provides a distinct compartment for hosting guest molecules. In contrast to conventional or ultralow cross-linked (ULC) microgels, where cargo is distributed throughout the polymer network, hollow microgels enable localization within a central void, which may help preserve the structure and activity of sensitive biomolecules such as proteins.

Experimental studies have demonstrated that hollow microgels can encapsulate proteins and nanoparticles, with uptake governed by a combination of electrostatic interactions, osmotic pressure, and shell permeability [38,138,142,143]. For instance, pH-responsive hollow microgels have been used to encapsulate cytochrome c, where both loading efficiency and spatial distribution can be tuned by adjusting the charge state of the protein and the microgel (Fig. 13A) [38]. At intermediate pH, electrostatic attraction promotes homogeneous loading, whereas at high or low pH, changes in charge and swelling state lead to redistribution of the protein between the shell and the cavity. Fluorescence lifetime imaging (FLIM) further reveals that the local environment of the encapsulated protein depends strongly on pH, reflecting variations in polymer density and hydration (Fig. 13B). These results demonstrate that hollow microgels act not only as passive containers, but as responsive microenvironments capable of tuning the localization and mobility of guest molecules.

However, these studies also highlight a fundamental limitation of hollow architectures. Even under favorable electrostatic conditions, only a fraction of the encapsulated protein is released upon external triggering, with a significant portion remaining trapped within the microgel [38]. This contrasts with conventional microgels, where cargo is more accessible and can be released more efficiently through swelling or charge reversal. The origin of this difference lies in the polymer shell, which acts as a semi-permeable barrier controlling transport into and out of the cavity. This barrier property is central to understanding the advantages and limitations of hollow microgels. On one hand, it enables confinement and protection of cargo, making hollow systems attractive for controlled release applications. On the other hand, it introduces an additional constraint for loading, which often requires diffusion through the shell or the presence of driving forces such as osmotic gradients or electrostatic attraction. In contrast, ULC microgels provide direct access to the network, allowing spontaneous uptake driven by equilibrium interactions.

Simulation studies provide further insights into these mechanisms [138]. In the swollen state, the release is primarily diffusion-controlled, as the increased mesh size facilitates transport through the shell (Fig. 13C). In contrast, during deswelling, rapid release can occur via convective flows as the shrinking of the capsule expels the solvent and entrained molecules. This highlights a key distinction between hollow and conventional microgels: while the latter rely predominantly on diffusive transport, hollow microgels can exploit the hydrodynamic effects associated with volume changes. Strategies to overcome these barrier limitations have also been proposed. For example, incorporating rigid inclusions within the cavity can prevent complete pore closure during deswelling (Fig. 13C(d)), thereby enhancing release efficiency [138]. More generally, tuning the mesh size, crosslinking density, and chemical functionality of the shell provides a route to control permeability and optimize transport properties.

Beyond single-shell systems, more sophisticated architectures have been developed to overcome transport limitations. Hollow shell–shell (HSS) nanogels, consisting of concentric thermoresponsive shells, provide an elegant strategy for controlled uptake and release [87,144]. These systems combine an inner PNIPAM shell (VPTT ≈ 32°C) and an outer PNIPMAM shell (VPTT ≈ 42°C), enabling temperature-controlled gating of the cavity. As illustrated in Fig. 14, guest molecules can diffuse into the swollen structure, become trapped upon collapse of the

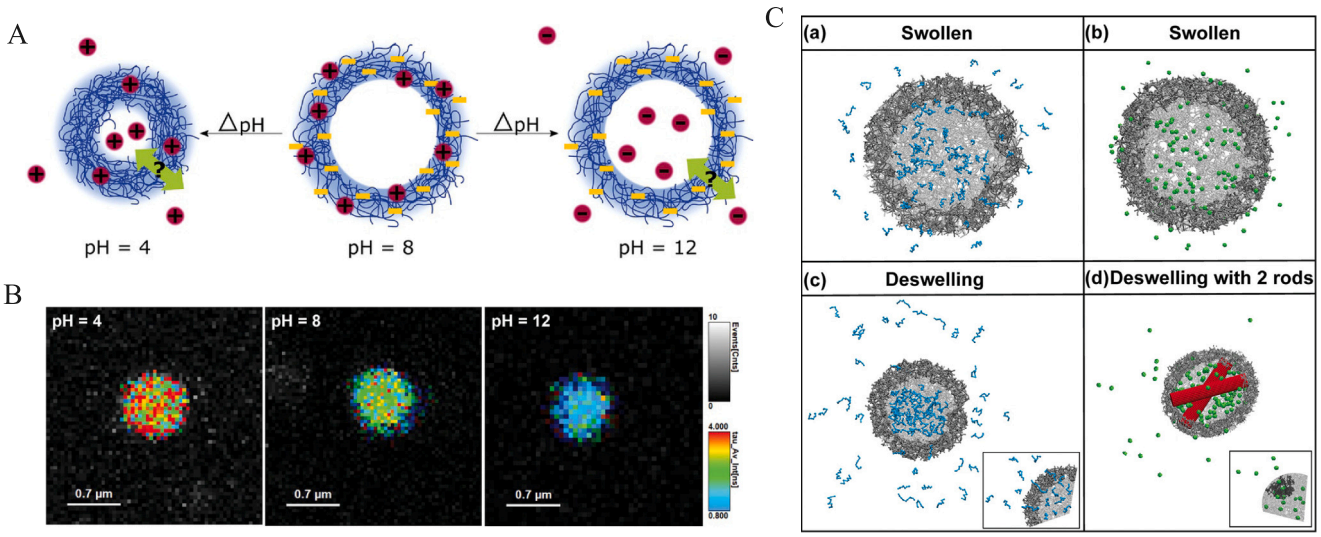

Fig. 13. (A) Schematic showing cytochrome c distribution within hollow anionic microgels: attraction at pH 8 enables encapsulation, repulsion at pH 12 prevents association, and charge neutralization at pH 4 leads to minimal interaction. (B) Spatial distribution of the lifetime-averaged intensity of the hollow anionic microgels loaded with labeled cytochrome c in buffers with the three respective pH values. Adapted with permission from Ref. [38]. (C) Panels a and b show simulation snapshots of polymer chains (cyan) and nanoparticles (green) released from the swollen gel capsules. Panels (c) and (d) show the release of these vesicles during deswelling: (c) without microrods and (d) with two free-moving microrods (red) inside. Cross-sectional views are shown; the solvent is omitted. Insets highlight polymer reptation (c) and nanoparticle discharge through the pores (d).
Source: Adapted with permission from Ref. [138].

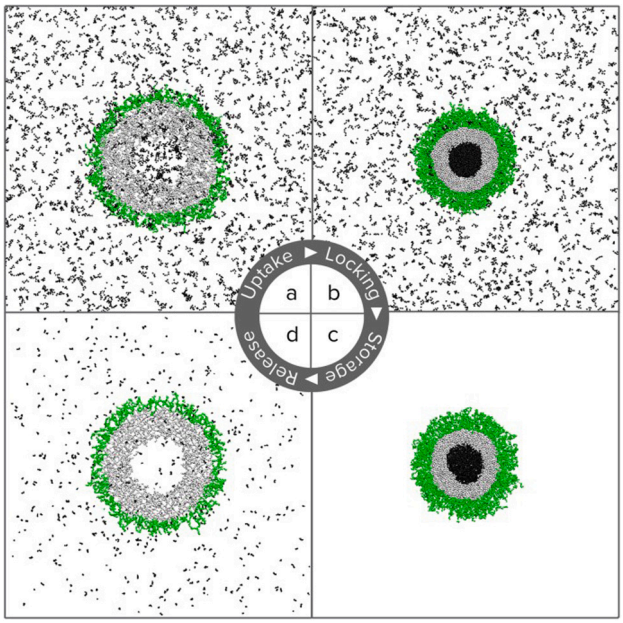

Fig. 14. Simulation snapshot of equilibrium structures of hollow shell–shell (HSS) nanogels with guest chains under different conditions: (a) Guest chains diffuse into the swollen nanogel; (b) Chains are locked inside as the inner shell collapses; (c) Collapsed inner shell holds the chains in the cavity; (d) Chains are released after the inner shell swells again.
Source: Reproduced with permission from Ref. [87].

inner shell, and be released again upon reswelling. This architecture decouples loading, confinement, and release, offering enhanced control over transport processes. An important aspect in evaluating hollow microgels as cargo carriers is therefore the role of the shell as a transport barrier. While the presence of a cavity suggests increased loading capacity, the surrounding polymer shell can significantly hinder uptake, making encapsulation dependent on permeability and network structure [41,87,145–147]. In contrast, ULC microgels exhibit open and highly accessible networks, where loading is governed by equilibrium polymer–guest interactions such as hydrophobic or electrostatic effects [28,148–150].

This distinction reflects fundamentally different loading mechanisms. In hollow microgels, encapsulation is often transport-limited and may require non-equilibrium strategies, such as loading under excess conditions followed by partial closure of the shell. In ULC systems, uptake is typically spontaneous and governed by thermodynamic equilibrium within the network [6,12,58,151]. Importantly, the presence of a barrier in hollow microgels, while limiting accessibility, provides a powerful handle for controlled release. Recent studies suggest that barrier properties can also be introduced *a posteriori* in initially open systems, for example through microgel–polyphenol interactions that induce the formation of denser outer layers [152–158]. Such approaches offer the possibility to combine facile loading with controlled retention.

As depicted in Fig. 15, a strategy of encapsulation is provided. As previously mentioned, ULC microgels provide an easy barrier-free way of cargo-loading in the polymer matrix, purely governed by polymer–drug interactions and permeability (Fig. 15A), opposite to hollow microgels, for which the encapsulation is limited by the polymer mesh dimensions and shell thickness (Fig. 15B). To account for this, a combined method could be implemented first, by benefiting for the high loading capacity of ULCs and then closing the structure with the introduction of a physical crosslinker in the system, such as tannic acid (Fig. 15C), protecting the loaded guest molecule that can be released by applying an external stimuli, e.g., ultrasonication [159].

Overall, hollow microgels present a trade-off between loading capacity and accessibility. While the cavity provides a defined compartment for encapsulation, the surrounding shell imposes constraints on transport that are absent in conventional or ULC microgels. Therefore, whether hollow microgels outperform alternative systems depends critically on the targeted application. The barrier properties of the shell are advantageous for applications requiring protection and controlled release. Conversely, for rapid uptake and release governed by molecular interactions, conventional microgels may remain more effective. These considerations raise a broader question: whether predefined hollow architectures are strictly required to achieve efficient encapsulation

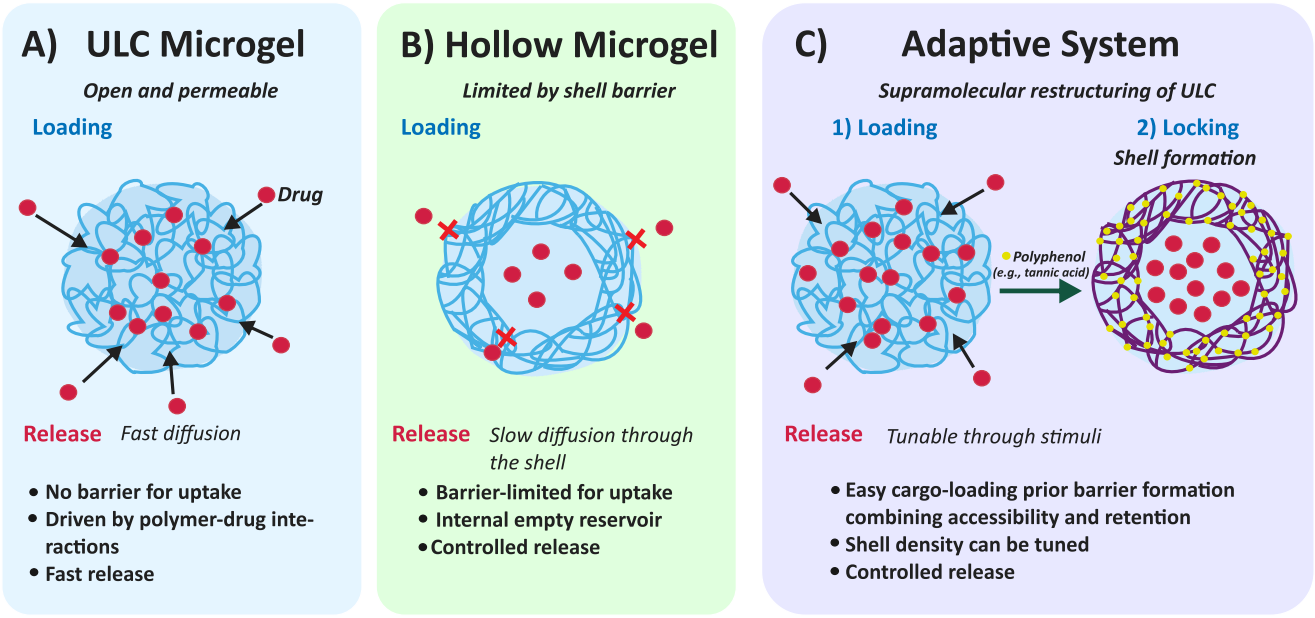

Fig. 15. Schematic illustration of cargo loading and release in ultralow crosslinked (ULC) microgels, hollow microgels, and supramolecularly structured microgels. (A) ULC microgels provide an open and highly permeable net, work enabling facile uptake but limited confinement. (B) Hollow microgels possess an internal cavity separated by a shell, leading to barrier-limited uptake but controlled release. (C) Supramolecular restructuring offers an adaptive approach, where cargo is first loaded into an open network and subsequently confined by the formation of a dense outer shell, combining accessibility and retention.

and controlled release, or whether comparable functionality can be obtained through adaptive or stimuli-induced restructuring of simpler microgel systems. Addressing this issue will be essential for determining when the additional synthetic complexity of hollow microgels is justified, and for guiding the design of next-generation responsive carriers.

8. Conclusions and future directions

Hollow nano/microgels have emerged as a highly versatile class of soft, stimuli-responsive materials with unique structural characteristics and broad application potential across fields ranging from drug delivery to advanced interface engineering. Their hallmark feature a solvent-filled cavity enclosed by a deformable polymer shell, introduces an additional degree of softness and internal freedom, enabling high loading capacities, tunable responsiveness, and complex mechanical behavior that is not accessible in conventional microgels.

This review has highlighted recent advances in the synthesis, structure, responsiveness, interfacial behavior, and applications of hollow microgels. A wide range of fabrication strategies, including sacrificial templating, microfluidics, layer-by-layer assembly, and emulsion-based approaches, now allow precise control over particle size, cavity geometry, shell thickness, and chemical functionality. These advances have enabled the systematic exploration of how hollow architecture influences both equilibrium properties and dynamic responses to external stimuli such as temperature, pH, ionic strength, and mechanical stress. A defining aspect of hollow microgels is their rich structural response under confinement and external stress. Compared to conventional microgels, hollow systems exhibit enhanced compressibility and additional deformation pathways arising from the presence of the cavity. At the nanoscale, deformation is primarily accommodated through inward polymer redistribution and cavity filling, whereas at larger length scales, thin shells can undergo reversible buckling transitions under osmotic stress. These distinct regimes highlight the central role of the core-to-shell ratio and shell mechanics in governing the transition between smooth deswelling and mechanical instability. At interfaces, hollow microgels display enhanced deformability and spreading, leading to adaptive interfacial assemblies with tunable packing and ordering. Their behavior reflects a balance between interfacial tension, shell elasticity, and internal architecture, placing them in an intermediate regime between soft polymer networks and elastic capsules. The introduction of anisotropy further enriches this behavior, enabling directional interactions, complex phase behavior, and structured assemblies both in bulk and at interfaces.

From an application perspective, hollow microgels offer unique opportunities in encapsulation, separation, catalysis, and membrane technologies. Their internal cavity enables compartmentalization and controlled transport, while the surrounding shell acts as a tunable barrier regulating permeability and release. This duality, combining accessibility with confinement, distinguishes hollow microgels from both conventional and ultralow crosslinked systems. At the same time, it introduces a fundamental trade-off between loading efficiency and transport, which must be carefully optimized depending on the targeted application. Despite significant progress, several key challenges and opportunities remain. A central objective for future research is the development of quantitative structure–property relationships that connect particle size, shell thickness, crosslinking density, and core-to-shell ratio with measurable properties such as elastic modulus, volume phase transition behavior, permeability, buckling thresholds, and cargo transport. In this context, the cavity should be regarded not merely as a geometric feature, but as a fundamental design parameter governing mechanical response, transport, and functionality.

Another important direction is the development of degradable, biocompatible [160–162], and ultimately bio-derived hollow microgels capsules [163]. While most current hollow-microgel model systems are based on synthetic polymers with comparatively well-controlled network architectures, soft colloidal networks can also be constructed from biopolymers such as proteins, polysaccharides, and other naturally derived macromolecules. These materials are often more heterogeneous and polydisperse than synthetic microgels, and their network elasticity and crosslink distribution may be more difficult to control quantitatively. Nevertheless, extending hollow architectures to such systems could be particularly valuable because biodegradability, biocompatibility, biochemical functionality, and enzymatic responsiveness are intrinsically encoded in many biopolymers. Future developments could

therefore enable hollow biopolymer microgels for controlled delivery, biomimetic compartments, encapsulation of biologically active species, food and formulation technologies, and environmentally degradable carriers. An important challenge will be to preserve a well-defined cavity and controllable shell mechanics while retaining the dynamic and degradable character of the biological network.

Finally, an important conceptual question emerging from this review is whether predefined hollow architectures are strictly required to achieve the desired functionality, or whether similar performance can be obtained through adaptive or stimuli-induced restructuring of simpler microgel systems. Addressing this question will be crucial for determining when the additional synthetic complexity of hollow microgels is justified, and for guiding the rational design of next-generation soft materials. Overall, hollow microgels represent a powerful platform in soft matter science, where geometry, mechanics, and responsiveness can be combined in a single object. Fully exploiting the hollow architecture as an independent design parameter will open new avenues toward programmable, adaptive, and multifunctional materials.

CRediT authorship contribution statement

Chandeshwar Misra: Writing – review & editing, Writing – original draft, Data curation, Conceptualization. **Alan O. Francisco-Mejia:** Writing – review & editing, Writing – original draft, Data curation. **Walter Richtering:** Writing – review & editing, Supervision, Funding acquisition, Conceptualization. **Jérôme J. Crassous:** Writing – review & editing, Writing – original draft, Supervision, Funding acquisition, Data curation, Conceptualization.

Declaration of Generative AI and AI-assisted technologies in the writing process

During the preparation of this work, the authors used ChatGPT (OpenAI) to assist with language editing, manuscript organization, and discussion of scientific concepts. All generated text was critically reviewed, revised, and verified by the authors, who take full responsibility for the content of this publication.

Declaration of competing interest

The authors declare that they have no known competing financial interests or personal relationships that could have appeared to influence the work reported in this paper.

Acknowledgments

The authors acknowledge financial support from the Deutsche Forschungsgemeinschaft (DFG) under grant No. CR 742/2-StarRAC (“Star and Amphiphilic Responsive Anisotropic Colloids: Design and Self-Assembly”) and from the Collaborative Research Center SFB 985 – Functional Microgels and Microgel Systems.

Data availability

No data was used for the research described in the article.

References

[1] Sigolaeva LV, Gladyr SY, Mergel O, Gelissen AP, Noyong M, Simon U, Pergushov DV, Kurochkin IN, Plamper FA, Richtering W. Easy-preparable butyrylcholinesterase/microgel construct for facilitated organophosphate biosensing. Anal Chem 2017;89(11):6091–8. http://dx.doi.org/10.1021/acs.analchem.7b00732.

[2] Pelton R. Temperature-sensitive aqueous microgels. Adv Colloid Interface Sci 2000;85(1):1–33. http://dx.doi.org/10.1016/S0001-8686(99)00023-8.

[3] Plamper FA, Richtering W. Functional microgels and microgel systems. Acc Chem Res 2017;50(2):131–40. http://dx.doi.org/10.1021/acs.accounts.6b00544.

[4] Dirksen M, Dargel C, Meier L, Brändel T, Hellweg T. Smart microgels as drug delivery vehicles for the natural drug aescin: Uptake, release and interactions. Colloid Polym Sci 2020;298:505–18. http://dx.doi.org/10.1007/s00396-020-04632-5.

[5] Dave R, Randhawa G, Kim D, Simpson M, Hoare T. Microgels and nanogels for the delivery of poorly water-soluble drugs. Mol Pharm 2022;19(6):1704–21. http://dx.doi.org/10.1021/acs.molpharmaceut.1c00967.

[6] Smeets NM, Hoare T. Designing responsive microgels for drug delivery applications. J Polym Sci A 2013;51(14):3027–43. http://dx.doi.org/10.1002/pola.26707.

[7] Klinger D, Landfester K. Stimuli-responsive microgels for the loading and release of functional compounds: Fundamental concepts and applications. Polymer 2012;53(23):5209–31. http://dx.doi.org/10.1016/j.polymer.2012.08.053.

[8] Sigolaeva LV, Gladyr SY, Gelissen AP, Mergel O, Pergushov DV, Kurochkin IN, Plamper FA, Richtering W. Dual-stimuli-sensitive microgels as a tool for stimulated spongelike adsorption of biomaterials for biosensor applications. Biomacromolecules 2014;15(10):3735–45. http://dx.doi.org/10.1021/bm5010349.

[9] Buenger D, Topuz F, Groll J. Hydrogels in sensing applications. Prog Polym Sci 2012;37(12):1678–719. http://dx.doi.org/10.1016/j.progpolymsci.2012.09.001.

[10] Ionov L. Hydrogel-based actuators: Possibilities and limitations. Mater Today 2014;17(10):494–503. http://dx.doi.org/10.1016/j.mattod.2014.07.002.

[11] Mourran A, Zhang H, Vinokur R, Möller M. Soft microrobots employing nonequilibrium actuation via plasmonic heating. Adv Mater 2017;29(2):1604825. http://dx.doi.org/10.1002/adma.201604825.

[12] Karg M, Pich A, Hellweg T, Hoare T, Lyon LA, Crassous J, Suzuki D, Gumerov RA, Schneider S, Potemkin II, et al. Nanogels and microgels: From model colloids to applications, recent developments, and future trends. Langmuir 2019;35(19):6231–55. http://dx.doi.org/10.1021/acs.langmuir.8b04304.

[13] Fernandez-Rodriguez MA, Martín-Molina A, Maldonado-Valderrama J. Microgels at interfaces, from mickering emulsions to flat interfaces and back. Adv Colloid Interface Sci 2021;288:102350. http://dx.doi.org/10.1016/j.cis.2020.102350.

[14] Senff H, Richtering W. Temperature sensitive microgel suspensions: Colloidal phase behavior and rheology of soft spheres. J Chem Phys 1999;111(4):1705–11. http://dx.doi.org/10.1063/1.479430.

[15] Brugnoni M, Nickel AC, Kröger LC, Scotti A, Pich A, Leonhard K, Richtering W. Synthesis and structure of deuterated ultra-low cross-linked poly (n-isopropylacrylamide) microgels. Polym Chem 2019;10(19):2397–405. http://dx.doi.org/10.1039/C8PY01699B.

[16] Hoare T, Pelton R. Highly ph and temperature responsive microgels functionalized with vinylacetic acid. Macromolecules 2004;37(7):2544–50. http://dx.doi.org/10.1021/ma035658m.

[17] Karg M, Pastoriza-Santos I, Rodriguez-Gonzalez B, von Klitzing R, Wellert S, Hellweg T. Temperature, ph, and ionic strength induced changes of the swelling behavior of pnipam- poly (allylacetic acid) copolymer microgels. Langmuir 2008;24(12):6300–6. http://dx.doi.org/10.1021/la702996p.

[18] Gelissen AP, Scotti A, Turnhoff SK, Janssen C, Radulescu A, Pich A, Rudov AA, Potemkin II, Richtering W. An anionic shell shields a cationic core allowing for uptake and release of polyelectrolytes within core–shell responsive microgels. Soft Matter 2018;14(21):4287–99. http://dx.doi.org/10.1039/C8SM00397A.

[19] Pinheiro J, Moura L, Fokkink R, Farinha J. Preparation and characterization of low dispersity anionic multiresponsive core–shell polymer nanoparticles. Langmuir 2012;28(13):5802–9. http://dx.doi.org/10.1021/la2045477.

[20] Daly E, Saunders BR. A study of the effect of electrolyte on the swelling and stability of poly (n-isopropylacrylamide) microgel dispersions. Langmuir 2000;16(13):5546–52. http://dx.doi.org/10.1021/la991292o.

[21] Chanda S, Misra C, Bandyopadhyay R. Investigating the roles of hydrophobicity and electrostatics in the particle-scale dynamics and rheology of dense microgel suspensions. J Appl Phys 2026;139(11):114701. http://dx.doi.org/10.1063/5.0309685.

[22] Scotti A, Schulte MF, Lopez CG, Crassous JJ, Bochenek S, Richtering W. How softness matters in soft nanogels and nanogel assemblies. Chem Rev 2022;122(13):11675–700. http://dx.doi.org/10.1021/acs.chemrev.2c00035.

[23] Conley GM, Zhang C, Aebischer P, Harden JL, Scheffold F. Relationship between rheology and structure of interpenetrating, deforming and compressing microgels. Nat Commun 2019;10(1):2436. http://dx.doi.org/10.1038/s41467-019-10181-5.

[24] Alsayed AM, Islam MF, Zhang J, Collings PJ, Yodh AG. Premelting at defects within bulk colloidal crystals. Science 2005;309(5738):1207–10. http://dx.doi.org/10.1126/science.1112399.

[25] Lyon LA, Fernandez-Nieves A. The polymer/colloid duality of microgel suspensions. Annu Rev Phys Chem 2012;63:25–43. http://dx.doi.org/10.1146/annurev-physchem-032511-143735.

[26] Petrunin AV, Höfken T, Schneider S, Mota-Santiago P, Houston JE, Scotti A. Phase behavior of binary mixtures of hollow and regular microgels. Soft Matter 2024;20:8125–35. http://dx.doi.org/10.1039/D4SM00862F.

[27] Brugnoni M, Fink F, Scotti A, Richtering W. Synthesis and structure of temperature-sensitive nanocapsules. Colloid Polym Sci 2020;298(9):1179–85. http://dx.doi.org/10.1007/s00396-020-04686-5.

[28] Hazra N, Lammertz J, Babenyshev A, Erkes R, Hagemans F, Misra C, Richtering W, Crassous JJ. Charged hollow microgel capsules. Soft Matter 2024;20:4608–20. http://dx.doi.org/10.1039/D4SM00111G.
[29] Rudov AA, Portnov IV, Bogdanova AR, Potemkin II. Structure of swollen hollow polyelectrolyte nanogels with inhomogeneous cross-link distribution. J Colloid Interface Sci 2023;640:1015–28. http://dx.doi.org/10.1016/j.jcis.2023.02.090.
[30] Gao H, Yang W, Min K, Zha L, Wang C, Fu S. Thermosensitive poly (n-isopropylacrylamide) nanocapsules with controlled permeability. Polymer 2005;46(4):1087–93. http://dx.doi.org/10.1016/j.polymer.2004.11.078.
[31] Bentz KC, Savin DA. Hollow polymer nanocapsules: Synthesis, properties, and applications. Polym Chem 2018;9(16):2059–81. http://dx.doi.org/10.1039/c8py00142a.
[32] Sakashita A, Urakami N, Ziherl P, Imai M. Three-dimensional analysis of lipid vesicle transformations. Soft Matter 2012;8:8569–81. http://dx.doi.org/10.1039/C2SM25759A.
[33] Quemeneur Fmc, Quilliet C, Faivre M, Viallat A, Pépin-Donat B. Gel phase vesicles buckle into specific shapes. Phys Rev Lett 2012;108:108303. http://dx.doi.org/10.1103/PhysRevLett.108.108303.
[34] Rideau E, Dimova R, Schwille P, Wurm FR, Landfester K. Liposomes and polymersomes: A comparative review towards cell mimicking. Chem Soc Rev 2018;47:8572–610. http://dx.doi.org/10.1039/C8CS00162F.
[35] Kansız S, Elçin YM. Advanced liposome and polymersome-based drug delivery systems: Considerations for physicochemical properties, targeting strategies and stimuli-sensitive approaches. Adv Colloid Interface Sci 2023;317:102930. http://dx.doi.org/10.1016/j.cis.2023.102930.
[36] Zha L, Zhang Y, Yang W, Fu S. Monodisperse temperature-sensitive microcontainers. Adv Mater 2002;14(15):1090–2. http://dx.doi.org/10.1002/1521-4095(20020805)14:15<1090::AID-ADMA1090>3.0.CO;2-6.
[37] Windbergs M, Zhao Y, Heyman J, Weitz DA. Biodegradable core–shell carriers for simultaneous encapsulation of synergistic actives. J Am Chem Soc 2013;135(21):7933–7. http://dx.doi.org/10.1021/ja401422r.
[38] Wypysek SK, Centeno SP, Gronemann T, Wöll D, Richtering W. Hollow, ph-sensitive microgels as nanocontainers for the encapsulation of proteins. Macromol Biosci 2023;2200456. http://dx.doi.org/10.1002/mabi.202200456.
[39] Seiffert S, Thiele J, Abate AR, Weitz DA. Smart microgel capsules from macromolecular precursors. J Am Chem Soc 2010;132(18):6606–9. http://dx.doi.org/10.1021/ja102156h.
[40] Nayak S, Gan DJ, Serpe MJ, Lyon L. Hollow thermoresponsive microgels. Small 2005;1(4):416–21. http://dx.doi.org/10.1002/smll.200400089.
[41] Tripathi BP, Dubey NC, Stamm M. Hollow microgel based ultrathin thermoresponsive membranes for separation, synthesis, and catalytic applications. ACS Appl Mater Interfaces 2014;6(20):17702–12. http://dx.doi.org/10.1021/am504120c, pMID: 25272373.
[42] Li G, Yang X, Wang B, Wang J, Yang X. Monodisperse temperature-responsive hollow polymer microspheres: Synthesis, characterization and biological application. Polymer 2008;49(16):3436–43. http://dx.doi.org/10.1016/j.polymer.2008.06.004.
[43] Xu X, Asher SA. Synthesis and utilization of monodisperse hollow polymeric particles in photonic crystals. J Am Chem Soc 2004;126(25):7940–5. http://dx.doi.org/10.1021/ja049453k.
[44] Peyratout CS, Dähne L. Tailor-made polyelectrolyte microcapsules: From multilayers to smart containers. Angew Chem Int Ed 2004;43(29):3762–83. http://dx.doi.org/10.1002/anie.200300568.
[45] Caruso F, Caruso RA, Möhwald H. Nanoengineering of inorganic and hybrid hollow spheres by colloidal templating. Science 1998;282(5391):1111–4. http://dx.doi.org/10.1126/science.282.5391.1111.
[46] Kim J-W, Utada AS, Fernández-Nieves A, Hu Z, Weitz DA. Fabrication of monodisperse gel shells and functional microgels in microfluidic devices. Angew Chem 2007;119(11):1851–4. http://dx.doi.org/10.1002/ange.200604206.
[47] Sun Q, Deng Y. In situ synthesis of temperature-sensitive hollow microspheres via interfacial polymerization. J Am Chem Soc 2005;127(23):8274–5. http://dx.doi.org/10.1021/ja051487k.
[48] Scotti A, Brugnoni M, Rudov AA, Houston JE, Potemkin II, Richtering W. Hollow microgels squeezed in overcrowded environments. J Chem Phys 2018;148(17):174903. http://dx.doi.org/10.1063/1.5026100.
[49] Scotti A, Denton AR, Brugnoni M, Schweins R, Richtering W. Absence of crystals in the phase behavior of hollow microgels. Phys Rev E 2021;103:022612. http://dx.doi.org/10.1103/PhysRevE.103.022612.
[50] Rank L, Zaccarelli E. Self-induced buckling in hollow microgels. ACS Nano 2026;20(4):3541–50. http://dx.doi.org/10.1021/acsnano.5c15990, pMID: 41537489.
[51] Hagemans F, Camerin F, Hazra N, Lammertz J, Dux F, Monte G Del, Laukkanen O-V, Crassous JJ, Zaccarelli E, Richtering W. Buckling and interfacial deformation of fluorescent poly (n-isopropylacrylamide) microgel capsules. ACS Nano 2023;17(8):7257–71. http://dx.doi.org/10.1021/acsnano.2c10164.
[52] Geisel K, Rudov AA, Potemkin II, Richtering W. Hollow and core–shell microgels at oil–water interfaces: Spreading of soft particles reduces the compressibility of the monolayer. Langmuir 2015;31(48):13145–54. http://dx.doi.org/10.1021/acs.langmuir.5b03530, pMID: 26575794.
[53] Vialetto J, Camerin F, Grillo F, Ramakrishna SN, Rovigatti L, Zaccarelli E, Isa L. Effect of internal architecture on the assembly of soft particles at fluid interfaces. ACS Nano 2021;15(8):13105–17. http://dx.doi.org/10.1021/acsnano.1c02486.
[54] Nickel AC, Rudov AA, Potemkin II, Crassous JJ, Richtering W. Interfacial assembly of anisotropic core–shell and hollow microgels. Langmuir 2022;38(14):4351–63. http://dx.doi.org/10.1021/acs.langmuir.2c00093.
[55] Hazra N, Rudov AA, Midya J, Babenyshev A, Bochenek S, Frenken M, Richtering W, Gompper G, Auth T, Potemkin II, et al. Capillary-driven self-assembly of soft ellipsoidal microgels at the air–water interface. Proc Natl Acad Sci 2024;121(52):e2403690121. http://dx.doi.org/10.1073/pnas.2403690121.
[56] Hagemans F, Hazra N, Lovasz VD, Awad AJ, Frenken M, Babenyshev A, Laukkanen O-V, Braunmiller D, Richtering W, Crassous JJ. Soft and deformable thermoresponsive hollow rod-shaped microgels. Small 2025;21(1):2401376. http://dx.doi.org/10.1002/smll.202401376.
[57] Dubbert J, Nothdurft K, Karg M, Richtering W. Core–shell–shell and hollow double-shell microgels with advanced temperature responsiveness. Macromol Rapid Commun 2015;36(2):159–64. http://dx.doi.org/10.1002/marc.201400495.
[58] Liu G, Zhu C, Xu J, Xin Y, Yang T, Li J, Shi L, Guo Z, Liu W. Thermo-responsive hollow silica microgels with controlled drug release properties. Colloids Surf B 2013;111:7–14. http://dx.doi.org/10.1016/j.colsurfb.2013.05.027.
[59] Lou XW, Archer LA, Yang Z. Hollow micro-/nanostructures: Synthesis and applications. Adv Mater 2008;20(21):3987–4019. http://dx.doi.org/10.1002/adma.200800854.
[60] Singh N, Lyon LA. Au nanoparticle templated synthesis of pnipam nanogels. Chem Mater 2007;19(4):719–26. http://dx.doi.org/10.1021/cm061878d.
[61] Stöber W, Fink A, Bohn E. Controlled growth of monodisperse silica spheres in the micron size range. J Colloid Interface Sci 1968;26(1):62–9. http://dx.doi.org/10.1016/0021-9797(68)90272-5.
[62] Zhang Y, Guan Y, Zhou S. Permeability control of glucose-sensitive nanoshells. Biomacromolecules 2007;8(12):3842–7. http://dx.doi.org/10.1021/bm700802p, pMID: 18020392.
[63] Wang Y, Liu Z, Peng H-Y, He F, Zhang L, Faraj Y, Wang W, Ju X-J, Xie R, Chu L-Y. A simple device based on smart hollow microgels for facile detection of trace lead(ii) ions. ChemPhysChem 2018;19(16):2025–36. http://dx.doi.org/10.1002/cphc.201800138.
[64] Sanson N, Rieger J. Synthesis of nanogels/microgels by conventional and controlled radical crosslinking copolymerization. Polym Chem 2010;1:965–77. http://dx.doi.org/10.1039/C0PY00010H.
[65] Utada AS, Lorenceau E, Link DR, Kaplan PD, Stone HA, Weitz D. Monodisperse double emulsions generated from a microcapillary device. Science 2005;308(5721):537–41. http://dx.doi.org/10.1126/science.1109164.
[66] Ikkai F, Iwamoto S, Adachi E, Nakajima M. New method of producing mono-sized polymer gel particles using microchannel emulsification and uv irradiation. Colloid Polym Sci 2005;283:1149–53. http://dx.doi.org/10.1007/s00396-005-1271-z.
[67] Cao Z, Ziener U, Landfester K. Synthesis of narrowly size-distributed thermosensitive poly (n-isopropylacrylamide) nanocapsules in inverse miniemulsion. Macromolecules 2010;43(15):6353–60. http://dx.doi.org/10.1021/ma101115t.
[68] Decher G, Schlenoff JB. Multilayer thin films: Sequential assembly of nanocomposite materials. Vol. 1, John Wiley & Sons; 2012, http://dx.doi.org/10.1002/3527600574.
[69] Wang Z, Feng Z, Gao C. Stepwise assembly of the same polyelectrolytes using host- guest interaction to obtain microcapsules with multiresponsive properties. Chem Mater 2008;20(13):4194–9. http://dx.doi.org/10.1021/cm8003358.
[70] Zhou L, Chen M, Tian L, Guan Y, Zhang Y. Release of polyphenolic drugs from dynamically bonded layer-by-layer films. ACS Appl Mater Interfaces 2013;5(9):3541–8. http://dx.doi.org/10.1021/am4008787.
[71] Johnston AP, Read ES, Caruso F. Dna multilayer films on planar and colloidal supports: Sequential assembly of like-charged polyelectrolytes. Nano Lett 2005;5(5):953–6. http://dx.doi.org/10.1021/nl050608b.
[72] Huang C-J, Chang F-C. Using click chemistry to fabricate ultrathin thermoresponsive microcapsules through direct covalent layer-by-layer assembly. Macromolecules 2009;42(14):5155–66. http://dx.doi.org/10.1021/ma900478n.
[73] Horecha M, Senkovskyy V, Stamm M, Kiriy A. One-pot synthesis of thermoresponsive pnipam hydrogel microcapsules designed to function in apolar media. Macromolecules 2009;42(15):5811–7. http://dx.doi.org/10.1021/ma9008934.
[74] Lu F, Luo Y, Li B, Zhao Q, Schork FJ. Synthesis of thermo-sensitive nanocapsules via inverse miniemulsion polymerization using a peo-raft agent. Macromolecules 2010;43(1):568–71. http://dx.doi.org/10.1021/ma902058b.
[75] Ninarello A, Crassous JJ, Paloli D, Camerin F, Gnan N, Rovigatti L, Schurtenberger P, Zaccarelli E. Modeling microgels with a controlled structure across the volume phase transition. Macromolecules 2019;52(20):7584–92. http://dx.doi.org/10.1021/acs.macromol.9b01122.
[76] Gnan N, Rovigatti L, Bergman M, Zaccarelli E. In silico synthesis of microgel particles. Macromolecules 2017;50(21):8777–86. http://dx.doi.org/10.1021/acs.macromol.7b01600.

[77] Hazra N, Ninarello A, Scotti A, Houston JE, Mota-Santiago P, Zaccarelli E, Crassous JJ. Structure of responsive microgels down to ultralow cross-linkings. Macromolecules 2024;57(1):339–55. http://dx.doi.org/10.1021/acs.macromol.3c00766.

[78] Wahrmund J, Kim J-W, Chu L-Y, Wang C, Li Y, Fernandez-Nieves A, Weitz DA, Krokhin A, Hu Z. Swelling kinetics of a microgel shell. Macromolecules 2009;42(23):9357–65. http://dx.doi.org/10.1021/ma901362p.

[79] Shaulli X, Rivas-Barbosa R, Bergman MJ, Zhang C, Gnan N, Scheffold F, Zaccarelli E. Probing temperature responsivity of microgels and its interplay with a solid surface by super-resolution microscopy and numerical simulations. ACS Nano 2023;17(3):2067–78. http://dx.doi.org/10.1021/acsnano.2c07569, pMID: 36656959.

[80] Nevskyi O, Wöll D. 3D super-resolution fluorescence imaging of microgels. Annu Rev Phys Chem 2023;74(Volume 74, 2023):391–414. http://dx.doi.org/10.1146/annurev-physchem-062422-022601.

[81] Scotti A, Denton AR, Brugnoni M, Houston JE, Schweins R, Potemkin II, Richtering W. Deswelling of microgels in crowded suspensions depends on cross-link density and architecture. Macromolecules 2019;52(11):3995–4007. http://dx.doi.org/10.1021/acs.macromol.9b00729.

[82] Schulte MF, Scotti A, Gelissen AP, Richtering W, Mourran A. Probing the internal heterogeneity of responsive microgels adsorbed to an interface by a sharp sfm tip: Comparing core–shell and hollow microgels. Langmuir 2018;34(14):4150–8. http://dx.doi.org/10.1021/acs.langmuir.7b03811.

[83] Schulte MF, Izak-Nau E, Braun S, Pich A, Richtering W, Göstl R. Microgels react to force: Mechanical properties, syntheses, and force-activated functions. Chem Soc Rev 2022;51:2939–56. http://dx.doi.org/10.1039/D2CS00011C.

[84] Dubbert J, Honold T, Pedersen JS, Radulescu A, Drechsler M, Karg M, Richtering W. How hollow are thermoresponsive hollow nanogels? Macromolecules 2014;47(24):8700–8. http://dx.doi.org/10.1021/ma502056y.

[85] Contreras-Cáceres R, Schellkopf L, Fernández-López C, Pastoriza-Santos I, Pérez-Juste J, Stamm M. Effect of the cross-linking density on the thermoresponsive behavior of hollow pnipam microgels. Langmuir 2015;31(3):1142–9. http://dx.doi.org/10.1021/la504176a.

[86] Brugnoni M, Scotti A, Rudov AA, Gelissen AP, Caumanns T, Radulescu A, Eckert T, Pich A, Potemkin II, Richtering W. Swelling of a responsive network within different constraints in multi-thermosensitive microgels. Macromolecules 2018;51(7):2662–71. http://dx.doi.org/10.1021/acs.macromol.7b02722.

[87] Schmid AJ, Dubbert J, Rudov AA, Pedersen JS, Lindner P, Karg M, Potemkin II, Richtering W. Multi-shell hollow nanogels with responsive shell permeability. Sci Rep 2016;6(1):22736. http://dx.doi.org/10.1038/srep22736.

[88] Berndt I, Pedersen JS, Richtering W. Structure of multiresponsive "intelligent" core- shell microgels. J Am Chem Soc 2005;127(26):9372–3. http://dx.doi.org/10.1021/ja051825h.

[89] Berndt I, Pedersen JS, Richtering W. Temperature-sensitive core–shell microgel particles with dense shell. Angew Chem Int Ed 2006;45(11):1737–41. http://dx.doi.org/10.1002/anie.200503888.

[90] Wypysek SK, Scotti A, Alziyadi MO, Potemkin II, Denton AR, Richtering W. Tailoring the cavity of hollow polyelectrolyte microgels. Macromol Rapid Commun 2020;41(1):1900422. http://dx.doi.org/10.1002/marc.201900422.

[91] Rank L, Zaccarelli E. Numerical insights on the volume phase transition of thermoresponsive hollow microgels. Soft Matter 2025;21:3979–90. http://dx.doi.org/10.1039/D5SM00057B.

[92] Scotti A, Gasser U, Petrunin AV, Fruhner L, Richtering W, Houston JE. Experimental determination of the bulk moduli of hollow nanogels. Soft Matter 2022;18(31):5750–8. http://dx.doi.org/10.1039/d2sm00680d.

[93] Wu J, Zhou B, Hu Z. Phase behavior of thermally responsive microgel colloids. Phys Rev Lett 2003;90(4):048304. http://dx.doi.org/10.1103/PhysRevLett.90.048304.

[94] Mohanty PS, Richtering W. Structural ordering and phase behavior of charged microgels. J Phys Chem B 2008;112(47):14692–7. http://dx.doi.org/10.1021/jp808203d.

[95] Misra C, Kawale SV, Behera SK, Bandyopadhyay R. Effect of particle stiffness on microgel self-assembly and suspension phase behavior over a broad temperature range. Phys Fluids 2024;36(10):103120. http://dx.doi.org/10.1063/5.0232833.

[96] Behera SK, Saha D, Gadige P, Bandyopadhyay R. Effects of polydispersity on the glass transition dynamics of aqueous suspensions of soft spherical colloidal particles. Phys Rev Mater 2017;1(5):055603. http://dx.doi.org/10.1103/PhysRevMaterials.1.055603.

[97] Roger K, Crassous JJ. How the interplay of molecular and colloidal scales controls drying of microgel dispersions. Proc Natl Acad Sci 2021;118(46):e2105530118. http://dx.doi.org/10.1073/pnas.2105530118.

[98] Franco S, Buratti E, Nigro V, Zaccarelli E, Ruzicka B, Angelini R. Glass and jamming rheology in soft particles made of PNIPAM and polyacrylic acid. Int J Mol Sci 2021;22(8):4032. http://dx.doi.org/10.3390/ijms22084032.

[99] Misra C, Gadige P, Bandyopadhyay R. Dichotomous behaviors of stress and dielectric relaxations in dense suspensions of swollen thermoreversible hydrogel microparticles. J Colloid Interface Sci 2023;630:223–31. http://dx.doi.org/10.1016/j.jcis.2022.10.002.

[100] Houston JE, Fruhner L, de la Cotte A, González J Rojo, Petrunin AV, Gasser U, Schweins R, Allgaier J, Richtering W, Fernandez-Nieves A, et al. Resolving the different bulk moduli within individual soft nanogels using small-angle neutron scattering. Sci Adv 2022;8(26):eabn6129. http://dx.doi.org/10.1126/sciadv.abn6129.

[101] Košmrlj A, Nelson DR. Statistical mechanics of thin spherical shells. Phys Rev X 2017;7:011002. http://dx.doi.org/10.1103/PhysRevX.7.011002.

[102] Gibson J. Linear elastic theory of thin shells(linear elastic theory of thin shells, considering membrane and bending theories of open and closed cylindrical shell). Oxford, Pergamon Press, Ltd.; 1965, 182 P (1965).

[103] Inman D, Kozlovskaya V, Nealy S, Nikishau P, Hossain MG, Kharlampieva E. Uniform reversible buckling in highly hydrated spherical ultrathin hydrogel shells. Macromol Rapid Commun 2025;46(16):2500257. http://dx.doi.org/10.1002/marc.202500257.

[104] Rank L, Moreno AJ, Zaccarelli E. Effective interactions and dynamical properties of thermoresponsive hollow microgels. Macromolecules 2026;59(15):8777–87. http://dx.doi.org/10.1021/acs.macromol.6c01002.

[105] Anakhov MV, Gumerov RA, Potemkin II. Enhanced scavenging of a minor component from mixtures of two immiscible liquids by hollow polymer microgels. Mol Syst Des Eng 2022;7(3):285–93. http://dx.doi.org/10.1039/d1me00152c.

[106] Destribats M, Lapeyre V, Wolfs M, Sellier E, Leal-Calderon F, Ravaine V, Schmitt V. Soft microgels as pickering emulsion stabilisers: Role of particle deformability. Soft Matter 2011;7(17):7689–98. http://dx.doi.org/10.1039/c1sm05240c.

[107] Wiese S, Tsvetkova Y, Daleiden NJ, Spieß AC, Richtering W. Microgel stabilized emulsions: Breaking on demand. Colloids Surfaces A 2016;495:193–9. http://dx.doi.org/10.1016/j.colsurfa.2016.02.003.

[108] Rey M, Hou X, Tang JSJ, Vogel N. Interfacial arrangement and phase transitions of pnipam microgels with different crosslinking densities. Soft Matter 2017;13(46):8717–27. http://dx.doi.org/10.1039/c7sm01558e.

[109] Johnson KL, Kendall K, Roberts A. Surface energy and the contact of elastic solids. Proc R Soc A 1971;324(1558):301–13. http://dx.doi.org/10.1098/rspa.1971.0141.

[110] Shi J, Müftü S, Wan K-T. Adhesion of an elastic convex shell onto a rigid plate. J Adhes 2011;87(6):579–94. http://dx.doi.org/10.1080/00218464.2011.583587.

[111] Bushuev NV, Gumerov RA, Rudov AA, Potemkin II. Compression and ordering of hollow microgels in monolayers formed at liquid–liquid interfaces. Langmuir 2023;39(35):12420–9. http://dx.doi.org/10.1021/acs.langmuir.3c01648.

[112] Style RW, Isa L, Dufresne ER. Adsorption of soft particles at fluid interfaces. Soft Matter 2015;11:7412–9. http://dx.doi.org/10.1039/C5SM01743B.

[113] Andreotti B, Snoeijer JH. Soft wetting and the shuttleworth effect, at the crossroads between thermodynamics and mechanics. Europhys Lett 2016;113(6):66001. http://dx.doi.org/10.1209/0295-5075/113/66001.

[114] Timoshenko SP, Woinowsky-Krieger S. Theory of plates and shells. 2nd ed. New York: McGraw-Hill; 1959.

[115] Landau LD, Lifshitz EM. Theory of elasticity. Course of theoretical physics, 3rd ed. vol. 7, Oxford: Pergamon Press; 1986.

[116] Vella D, Ajdari A, Vaziri A, Boudaoud A. The indentation of pressurized elastic shells: From polymeric capsules to yeast cells. J R Soc Interface 2012;9(68):448–55. http://dx.doi.org/10.1098/rsif.2011.0352.

[117] Knoche S, Kierfeld J. Buckling of spherical capsules. Phys Rev E 2011;84:046608. http://dx.doi.org/10.1103/PhysRevE.84.046608.

[118] Nickel AC, Denton AR, Houston JE, Schweins R, Plivelic TS, Richtering W, Scotti A. Beyond simple self-healing: How anisotropic nanogels adapt their shape to their environment. J Chem Phys 2022;157(19):194901. http://dx.doi.org/10.1063/5.0119527.

[119] Kudryashova SS, Gumerov RA, Anakhov MV, Nemchenko VA, Potemkin II. Amphiphilic hollow microgels at the liquid–liquid interface: Studying soft colloids' shape and interior via computer simulations and machine learning. Langmuir 2026;42(23):16704–19. http://dx.doi.org/10.1021/acs.langmuir.6c01435, arXiv:https://pubs.acs.org/langd5/article-pdf/42/23/16704/66274363/acs.langmuir.6c01435.pdf.

[120] Frenkel D. Structure of hard-core models for liquid crystals. J Phys Chem 1988;92(11):3280–4. http://dx.doi.org/10.1021/j100322a042.

[121] McGrother SC, Williamson DC, Jackson G. A re-examination of the phase diagram of hard spherocylinders. J Chem Phys 1996;104(17):6755–71. http://dx.doi.org/10.1063/1.471343.

[122] Kuijk A, Byelov DV, Petukhov AV, Blaaderen A Van, Imhof A. Phase behavior of colloidal silica rods. Faraday Discuss 2012;159(1):181–99. http://dx.doi.org/10.1039/c2fd20084h.

[123] Zholudev SI, Gumerov RA, Larina AA, Potemkin II. Swelling, collapse and ordering of rod-like microgels in solution: Computer simulation studies. J Colloid Interface Sci 2023;629:270–8. http://dx.doi.org/10.1016/j.jcis.2022.09.050.

[124] Kuijk A, Blaaderen A Van, Imhof A. Synthesis of monodisperse, rodlike silica colloids with tunable aspect ratio. J Am Chem Soc 2011;133(8):2346–9. http://dx.doi.org/10.1021/ja109524h.

[125] Besseling T, Hermes M, Kuijk A, Nijs B De, Deng T, Dijkstra M, Imhof A, Blaaderen A Van. Determination of the positions and orientations of concentrated rod-like colloids from 3d microscopy data. J Phys: Condens Matter 2015;27(19):194109. http://dx.doi.org/10.1088/0953-8984/27/19/194109.

[126] Hagemans F, Pujala RK, Hotie DS, Thies-Weesie DM, de Winter DM, Meeldijk JD, Blaaderen A Van, Imhof A. Shaping silica rods by tuning hydrolysis and condensation of silica precursors. Chem Mater 2018;31(2):521–31. http://dx.doi.org/10.1021/acs.chemmater.8b04607.

[127] Crassous JJ, Dietsch H, Pfleiderer P, Malik V, Diaz A, Hirshi LA, Drechsler M, Schurtenberger P. Preparation and characterization of ellipsoidal-shaped thermosensitive microgel colloids with tailored aspect ratios. Soft Matter 2012;8(13):3538–48. http://dx.doi.org/10.1039/c2sm07257b.

[128] Crassous JJ, Mihut AM, Wernersson E, Pfleiderer P, Vermant J, Linse P, Schurtenberger P. Field-induced assembly of colloidal ellipsoids into well-defined microtubules. Nat Commun 2014;5(1):5516. http://dx.doi.org/10.1038/ncomms6516.

[129] Crassous JJ, Mihut AM, Månsson LK, Schurtenberger P. Anisotropic responsive microgels with tuneable shape and interactions. Nanoscale 2015;7(38):15971–82. http://dx.doi.org/10.1039/c5nr03827h.

[130] Krüger AJ, Bakirman O, Guerzoni LP, Jans A, Gehlen DB, Rommel D, Haraszti T, Kuehne AJ, Laporte L De. Compartmentalized jet polymerization as a high-resolution process to continuously produce anisometric microgel rods with adjustable size and stiffness. Adv Mater 2019;31(49):1903668. http://dx.doi.org/10.1002/adma.201903668.

[131] Wolff HJ, Linkhorst J, Göttlich T, Savinsky J, Krüger AJ, Laporte L De, Wessling M. Soft temperature-responsive microgels of complex shape in stop-flow lithography. Lab Chip 2020;20(2):285–95. http://dx.doi.org/10.1039/c9lc00749k.

[132] Saadli M, Braunmiller DL, Mourran A, Crassous JJ. Thermally and magnetically programmable hydrogel microactuators. Small 2023;19(16):2207035. http://dx.doi.org/10.1002/smll.202207035.

[133] Yang Z, Muller AH, Xu C, Doyle PS, DeSimone JM, Lahann J, Sciortino F, Glotzer S, Hong L, Aarts DA, et al. Janus particle synthesis, self-assembly and applications. R Soc Chem 2012. http://dx.doi.org/10.1039/9781849735100.

[134] Braunmiller DL, Babu S, Gehlen DB, Seuß M, Haraszti T, Falkenstein A, Eigen J, Laporte L De, Crassous JJ. Pre-programmed rod-shaped microgels to create multi-directional anisogels for 3d tissue engineering. Adv Funct Mater 2022;32(50):2202430. http://dx.doi.org/10.1002/adfm.202202430.

[135] Nickel AC, Scotti A, Houston JE, Ito T, Crassous J, Pedersen JS, Richtering W. Anisotropic hollow microgels that can adapt their size, shape, and softness. Nano Lett 2019;19(11):8161–70. http://dx.doi.org/10.1021/acs.nanolett.9b03507.

[136] Städele V, Gasser U, Dietsch H. Ellipsoidal hybrid magnetic microgel particles with thermally tunable aspect ratios. Soft Matter 2012;8(16):4427–31. http://dx.doi.org/10.1039/c2sm07152e.

[137] Lehle H, Noruzifar E, Oettel M. Ellipsoidal particles at fluid interfaces. Eur Phys J E 2008;26:151–60. http://dx.doi.org/10.1140/epje/i2007-10314-1.

[138] Masoud H, Alexeev A. Controlled release of nanoparticles and macromolecules from responsive microgel capsules. ACS Nano 2012;6(1):212–9. http://dx.doi.org/10.1021/nn2043143.

[139] Hassan A, Sajid I, Akmal M, Aslam M, Roy PG, Zhou S, Irfan A, Shahid M, Begum R, Farooqi ZH. Hollow microgels and their hybrids: Classification, synthesis, characterization, properties and applications. Rev Chem Eng 2024;40(3):377–400. http://dx.doi.org/10.1515/revce-2022-0074.

[140] Song X, Bao B, Tao J, Zhao S, Han X, Liu H. Deswelling dynamics of thermoresponsive microgel capsules and their ultrasensitive sensing applications: A mesoscopic simulation study. J Phys Chem C 2018;123(3):1828–38. http://dx.doi.org/10.1021/acs.jpcc.8b09998.

[141] Yang X, Chen L, Huang B, Bai F, Yang X. Synthesis of ph-sensitive hollow polymer microspheres and their application as drug carriers. Polymer 2009;50(15):3556–63. http://dx.doi.org/10.1016/j.polymer.2009.06.027.

[142] Hajebi S, Abdollahi A, Roghani-Mamaqani H, Salami-Kalajahi M. Temperature-responsive poly (n-isopropylacrylamide) nanogels: The role of hollow cavities and different shell cross-linking densities on doxorubicin loading and release. Langmuir 2020;36(10):2683–94. http://dx.doi.org/10.1021/acs.langmuir.9b03892.

[143] Moncho-Jorda A, Germán-Bellod A, Angioletti-Uberti S, Adroher-Benítez I, Dzubiella J. Nonequilibrium uptake kinetics of molecular cargo into hollow hydrogels tuned by electrosteric interactions. ACS Nano 2019;13(2):1603–16. http://dx.doi.org/10.1021/acsnano.8b07609.

[144] Richtering W, Potemkin II, Rudov AA, Sellge G, Trautwein C. Could multiresponsive hollow shell–shell nanocontainers offer an improved strategy for drug delivery? Nanomedicine 2016;11(22):2879–83. http://dx.doi.org/10.2217/nnm-2016-0327.

[145] Saunders BR, Vincent B. Microgel particles as model colloids: Theory, properties and applications. Adv Colloid Interface Sci 1999;80(1):1–25. http://dx.doi.org/10.1016/S0001-8686(98)00071-2.

[146] Agrawal G, Ülpenich A, Zhu X, Möller M, Pich A. Microgel-based adaptive hybrid capsules with tunable shell permeability. Chem Mater 2014;26(20):5882–91. http://dx.doi.org/10.1021/cm502358s.

[147] Lapeyre V, Renaudie N, Dechezelles J-F, Saadaoui H, Ravaine S, Ravaine V. Multiresponsive hybrid microgels and hollow capsules with a layered structure. Langmuir 2009;25(8):4659–67. http://dx.doi.org/10.1021/la9003438.

[148] Bachman H, Brown AC, Clarke KC, Dhada KS, Douglas A, Hansen CE, Herman E, Hyatt JS, Kodlekere P, Meng Z, et al. Ultrasoft, highly deformable microgels. Soft Matter 2015;11(10):2018–28. http://dx.doi.org/10.1039/c5sm00047e.

[149] Scotti A, Brugnoni M, Lopez CG, Bochenek S, Crassous JJ, Richtering W. Flow properties reveal the particle-to-polymer transition of ultra-low crosslinked microgels. Soft Matter 2020;16(3):668–78. http://dx.doi.org/10.1039/c9sm01451a.

[150] Douglas AM, Fragkopoulos AA, Gaines MK, Lyon LA, Fernandez-Nieves A, Barker TH. Dynamic assembly of ultrasoft colloidal networks enables cell invasion within restrictive fibrillar polymers. Proc Natl Acad Sci USA 2017;114(5):885–90. http://dx.doi.org/10.1073/pnas.1607350114.

[151] Agrawal G, Agrawal R. Functional microgels: Recent advances in their biomedical applications. Small 2018;14(39):1801724. http://dx.doi.org/10.1002/smll.201801724.

[152] Xu J, Liu X, Liang P, Yuan H, Yang T. In situ preparation of tannic acid-modified poly (n-isopropylacrylamide) hydrogel coatings for boosting cell response. Pharmaceutics 2024;16(4):538. http://dx.doi.org/10.3390/pharmaceutics16040538.

[153] Xue J, Ji W, Dong S, Zhang Z, Gao J, Yang P, Nie J, Du B. Degradable and thermosensitive microgels with tannic acid as the sole cross-linker. Langmuir 2019;35(49):16353–65. http://dx.doi.org/10.1021/acs.langmuir.9b03112.

[154] Ok S, Altun A. Interactions of poly (vinyl alcohol) and poly (n-isopropylacrylamide) with tannic acid and pyrazole derivatives: The identification of h-bonds for revealing a “two-molecules” carrier system. Eur Polym J 2018;108:472–84. http://dx.doi.org/10.1016/j.eurpolymj.2018.09.028.

[155] Costa E, Coelho M, Ilharco LM, Aguiar-Ricardo A, Hammond PT. Tannic acid mediated suppression of pnipaam microgels thermoresponsive behavior. Macromolecules 2011;44(3):612–21. http://dx.doi.org/10.1021/ma1025016.

[156] Chen G, Niu CH, Zhou M-Y, Ju X-J, Xie R, Chu L-Y. Phase transition behaviors of poly (n-isopropylacrylamide) microgels induced by tannic acid. J Colloid Interface Sci 2010;343(1):168–75. http://dx.doi.org/10.1016/j.jcis.2009.11.047.

[157] López CM, Pich A. Supramolecular stimuli-responsive microgels crosslinked by tannic acid. Macromol Rapid Commun 2018;39(6):1700808. http://dx.doi.org/10.1002/marc.201700808.

[158] Zhou J, Lin Z, Ju Y, Rahim MA, Richardson JJ, Caruso F. Polyphenol-mediated assembly for particle engineering. Acc Chem Res 2020;53(7):1269–78. http://dx.doi.org/10.1021/acs.accounts.0c00150.

[159] Petrunin AV, Braun S, Byn FJ, Milvydaité I, Kratzenberg T, Mota-Santiago P, Scotti A, Pich A, Richtering W. Unraveling the mechanisms of ultrasound-induced mechanical degradation of microgels: Effects of mechanoresponsive crosslinks, softness, and core–shell architecture. 2026, arXiv preprint arXiv:2601.13862.

[160] Farjami T, Madadlou A. Fabrication methods of biopolymeric microgels and microgel-based hydrogels. Food Hydrocolloids 2017;62:262–72. http://dx.doi.org/10.1016/j.foodhyd.2016.08.017.

[161] Akgonullu DZ, Murray BS, Connell SD, Fang Y, Linter B, Sarkar A. Synthetic and biopolymeric microgels: Review of similarities and difference in behaviour in bulk phases and at interfaces. Adv Colloid Interface Sci 2023;320:102983. http://dx.doi.org/10.1016/j.cis.2023.102983.

[162] McClements DJ. Designing biopolymer microgels to encapsulate, protect and deliver bioactive components: Physicochemical aspects. Adv Colloid Interface Sci 2017;240:31–59. http://dx.doi.org/10.1016/j.cis.2016.12.005.

[163] Schüler C, Caruso F. Decomposable hollow biopolymer-based capsules. Biomacromolecules 2001;2(3):921–6. http://dx.doi.org/10.1021/bm010052w.